
QUAECUMQUE VERA

THE UNIVERSITY OF ALBERTA

RELEASE FORM

NAME OF AUTHOR: R.L. SINCLAIR

TITLE OF THESIS: RADIO FREQUENCY EXCITED CO_2 GAS WAVEGUIDE LASERS

DEGREE FOR WHICH THESIS WAS PRESENTED: MASTER OF SCIENCE

YEAR THIS DEGREE GRANTED: 1984

THE UNIVERSITY OF ALBERTA

RADIO FREQUENCY EXCITED CO_2 GAS WAVEGUIDE LASERS

by

R.L. SINCLAIR

A THESIS
SUBMITTED TO THE FACULTY OF GRADUATE STUDIES AND RESEARCH
IN PARTIAL FULFILMENT OF THE REQUIREMENTS FOR THE DEGREE
OF MASTER OF SCIENCE

THE DEPARTMENT OF ELECTRICAL ENGINEERING

EDMONTON, ALBERTA
SPRING 1984

THE UNIVERSITY OF ALBERTA

FACULTY OF GRADUATE STUDIES AND RESEARCH

The undersigned certify that they have read, and recommend to the Faculty of Graduate Studies and Research, for acceptance, a thesis entitled

RADIO FREQUENCY EXCITED CO_2 GAS WAVEGUIDE LASERS

submitted by R.L. SINCLAIR

in partial fulfilment of the requirements for the degree of Master of Science.

ABSTRACT

This thesis describes the construction of radio frequency excited carbon dioxide waveguide lasers. The results of this work may be divided into three areas where significant accomplishments have been achieved.

Radio frequency discharge experiments were used to investigate several potential impedance matching techniques. The effect of the R.F. source frequency, the input power density and the gas mixture on the discharge voltage were also examined. A single pass hybrid waveguide was assembled and aligned to operate as a single pass laser. Such parameters as output coupler reflectivity, channel size and gas mixture were examined with this device. A double pass homogeneous waveguide was constructed and aligned for both single and double pass operation. The effect of alignment and input power density upon the output power and transverse mode stability were tested with this device. Throughout this work the importance of efficient gas excitation together with a compact design was emphasized.

ACKNOWLEDGEMENTS

I would like to express my thanks to Dr. J. Tulip for his guidance and support in this work.

I wish also to thank G. Fij for his technical skills, without which, the discharge structures and lasers could not have been built.

TABLE OF CONTENTS

CHAPTER PAGE

1. INTRODUCTION 1

2. THEORETICAL CONSIDERATIONS

2.1 Output Power 5

2.2 Importance of Cooling 7

2.3 Optical Losses 10

2.4 Transverse Mode Discrimination and Stability 17

2.5 Power Supply Operating Frequency 18

2.6 Design Criteria 23

3. THE R.F. DISCHARGE EXPERIMENTS

3.1 Construction of the Discharge Structures 26

3.2 Experiments 29

3.3 Modeling the Discharge 33

3.4 Hybrid Discharge Structure 34

4. THE 20 WATT WAVEGUIDE LASER

4.1 Construction Details 49

4.2 Operation and Behaviour 52

5. THE FOLDED WAVEGUIDE CAVITY

5.1 Construction Details 59

5.2 Laser Operation 62

6. CONCLUSIONS AND RECOMMENDATIONS 70

7. REFERENCES 73

LIST OF TABLES

TABLE	DESCRIPTION	PAGE
2-1	Thermal Conductivity and Linear Expansion Coefficients	9
2-2	Calculated Temperature Gradients	9
2-3	Dielectric Constants of the Waveguide Materials	13
2-4	Theoretical Absorption Losses	14
2-5	Bending Radius Required to Double Optical Absorption	16
2-6	Electrical Properties of Three Waveguide Materials	22
2-7	High Power CW Carbon Dioxide Waveguide Lasers	24
3-1	Standing Voltage Variation as the R.F. Source Frequency Increases	35
3-2	Standing Voltage Variation as the Number of Inductors is Increased	37
3-3	Standing Voltage Variation as the Electrode is Shortened	39

LIST OF FIGURES

FIGURE	DESCRIPTION	PAGE
2-1	Geometry used for Temperature Gradient Calculations	8
2-2	Geometry of a Hollow Rectangular Guide	12
2-3	Geometry used to Calculate Bending Losses	16
2-4	Microstripline Geometry	21
3-1	A Schematic of the Discharge Structure	27
3-2	A Schematic of the Experimental Apparatus	28
3-3	Typical Matching Networks	30
3-4	R.F. Amplifier Output Power versus Time	32
3-5	Electrode Voltage Profiles as the Source Frequency Increases	36
3-6	Electrode Voltage Profiles as the Number of Inductors is Increased	38
3-7	Cross Sectional View of the Hybrid Discharge Structure	41
3-8	Variation of Voltage and E/P Ratio Versus Gas Pressure	42
3-9	Variation of Discharge Voltage with Current	44
3-10	Variation of Discharge Voltage with Input Power Density	45
3-11	Discharge Voltage versus Input Power Density	46
4-1a	The 20 Watt Waveguide Laser	50
4-1b	The Waveguide Laser with Matching Networks Removed	50
4-2	The Laser Waveguide Channel	51
4-3	Laser Output Power versus Gas Pressure	53
4-4	Laser Output Power versus Output Coupler Reflectivity	55

LIST OF FIGURES (Cont'd)

FIGURE	DESCRIPTION	PAGE
4-5	Laser Output Power versus Gas Pressure for a 2.0 mm Square Bore	56
5-1a	Top View of the Folded Cavity Waveguide	61
5-1b	Schematic of the Waveguide Cross Section	61
5-2a	The Folded Cavity Carbon Dioxide Waveguide Laser	63
5-2b	External View of the Waveguide Laser with Matching Networks Removed	63
5-3	Two Geometries used as a Single Channel Laser	64
5-4	Laser Output Power versus Gas Pressure	66
5-5	Laser Power and Efficiency versus Input Power	67
5-6	Laser Output Power versus Gas Pressure	68

LIST OF SYMBOLS

SYMBOL	DEFINITION
CW	Continuous wave
R.F.	Radio frequency
D.C.	Direct current
Po	Laser output power
t	Transmission loss
g_o	Small signal gain
I_s	Saturation intensity
v_o	Line center frequency
t_μ, t_ℓ	Lifetimes of upper and lower laser levels
σ_o	Cross section for stimulated emission
A	Area of mode
ℓ	Active gain length
L	Distributed passive loss
k_w	Thermal conductivity of waveguide
r_1, r_2	Inner and outer radii of a cylindrical waveguide
ΔT	Temperature gradient
α	Absorption coefficient
λ	Wavelength of laser radiation
R	Radius of curvature of guide
d	Distance of optic from guide
k	$2\pi/\lambda$
R_D	The equivalent discharge resistance
C	The capacitance of the laser head
R_S	The equivalent resistance of the matching network.

CHAPTER 1

INTRODUCTION

The concept of a waveguide gas laser was first proposed, in 1964, by Marcatili and Schmeltzer [1] in a paper discussing the waveguiding properties of hollow dielectric tubes. Four years later this concept was independently reintroduced by Steffen and Kneubuhl [2] to explain anomalies, observed by Schwaller et al. [3], in the transverse mode structure of a HCN laser. In 1971, Smith [4] demonstrated the first operation of a waveguide gas laser. This HeNe laser was constructed with a 430-µm diameter glass capillary tube and its fabrication signalled the beginning of the development of waveguide laser technology. In 1972, Bridges et al. [5] assembled the first CO_2 gas waveguide laser. In this system mixtures of helium, carbon dioxide and nitrogen were flowed through a one millimeter diameter glass capillary tube to yield a maximum of 1.4 watts of CW laser radiation.

Radio frequency power sources were first used in connection with lasers to excite HeNe gas mixtures [6,7]. In 1965, R.F. excitation was employed to excite a CO_2 gas laser [8]. However, R.F. excited gas discharges were not new. Francis [9] provides an excellent review of the properties of R.F. excited gas discharges which were investigated for over 20 years prior to their application to lasers.

The special stability of R.F. discharges was employed by Crocker and Willis [10], who found that it was not possible to produce a uniform plasma in their CW co-axial laser using only D.C. excitation. They combined a D.C. supply and a R.F. power supply, which operated at 6, 36 or 90 MHz, to obtain a stable CW discharge. Pulsed, R.F. assisted, D.C. discharges have also been employed to produce high output power carbon dioxide lasers [11,12].

Finally, in 1976, transverse radio frequency excitation and waveguide laser technology were combined to produce a R.F. excited carbon dioxide waveguide laser [13,14]. Subsequent examination of these R.F. discharges revealed that R.F. excited waveguide lasers were potentially very efficient and reliable devices [15,16].

The R.F. discharge exhibits a positive impedance characteristic and does not include a cathode fall region. The positive impedance allows the elimination of ballast resistors. These resistors are used in conventional D.C. discharges to limit the discharge current and hence, prevent arcing. This resistive ballast used in a conventional discharge consumes a great deal of power so that its elimination leads to a potentially greater electrical efficiency. Even further gains in efficiency are realizable, since R.F. discharges are sustained by slightly lower electric fields [16] than comparable D.C. discharges. This lower electric field allows the realization of a more optimum field/pressure (E/P) ratio.

The absence of the cathode fall region permits a transverse R.F. discharge structure to be employed. In a D.C. discharge such a geometry cannot be employed because the discharge would collapse into a series of arcs. These arcs localize the electron excitation and lead to degradation of the laser performance. In addition, this transverse discharge can be produced by electrodes external to the discharge since the R.F. power can be capacitively coupled, through an insulating layer, into the channel. The elimination of the internal electrodes removes a major source of contamination which often reduces the laser lifetime. However, even if internal electrodes remained, the laser reliability would still be enhanced because the R.F. fields, due to the absence of the cathode fall, would be insufficient to produce a significant amount of electrode erosion.

A further advantage of a R.F. excited laser is that it can be scaled to yield higher CW output powers with greater ease than a D.C. excited laser. Under normal operating conditions a D.C. waveguide laser requires over 1.0 kV of drive voltage per centimeter of discharge [16]. Because of the difficulty of handling voltages much greater than 10 kV in non-laboratory environments, lasers longer than several centimeters require two or more discharge segments. The negative impedance of such a discharge requires that each discharge section be separately ballasted. Even with independent ballasting, independent starting circuitry, and large gaps between discharge sections, the following problems tend to occur:

a) Lighting and maintaining separate independent discharges is difficult;

b) There is a tendency for a discharge to occur between discharge legs;

c) Mirror mounts may float at high voltage.

In contrast, a R.F. excited gas discharge is transverse and so it can be lengthened by increasing only the supply current and not the supply voltage. Therefore, a R.F. excited carbon dioxide waveguide laser is potentially a very compact, efficient and reliable device. Coincidently these characteristics are precisely those required by a carbon dioxide laser so that it can be used for surgical applications. Presently such a surgical device is commercially available [17]. However, it produces only 20 watts of laser power, which is not sufficient for all types of surgery.

For example, Lobraico [18] suggests that a maximum output power of 50 watts would be useful in gynecological surgery while Nimsakul [66] indicates that 30-40 watts of power is required to perform kidney, liver, lung and brain surgery. At present, the largest commercially available R.F. excited carbon dioxide waveguide laser provides only 30 watts of power. Therefore, the purpose of the work described in this report was to study R.F. excited carbon dioxide waveguide

lasers so as to acquire the knowledge and technical expertise required to build an efficient and powerful carbon dioxide waveguide laser.

This study, as reported in Chapters 2 and 3, included theoretical calculations and numerous discharge experiments. These investigations were used to assess such parameters as the waveguide material, the impedance matching network, the waveguide geometry, the resonator configuration and the R.F. source frequency. Chapter 4 examines a 20 watt waveguide laser which yielded information on transverse mode stability, optimum channel size and the effects of optical losses. Lastly, a folded geometry was employed to produce a compact powerful laser. Chapter 5 considers this design which yielded a maximum of 30 watts at 10% efficiency. The experiments also emphasized the importance of reducing the scattering losses and preventing contamination of the alumina waveguide. Overall, the project provided a solid base of knowledge and indicated that a R.F. excited carbon dioxide waveguide laser which produces more than 30 watts of power can be built.

CHAPTER 2

THEORETICAL CONSIDERATIONS

This chapter examines the design of gas waveguide lasers. A variety of sources, both theoretical and experimental, were consulted from which the parameters which influence the laser's performance were identified. Once identified, a set of optimum values were proposed. Subsequent experimental work (see Chapters 3 to 5) was then used to assess the accuracy of these choices.

2.1 Output Power

Gas waveguide lasers usually operate at gas pressures equal to or greater than 100 Torr [19]. In this pressure broadened regime, Rigrod's power equation [20] can be used to predict the laser output power.

$$P_o = \frac{t}{t + L} I_s A g_o \ell (1 - \frac{t + L}{2 g_o \ell}) \qquad (2-1)$$

This equation was derived by applying the simplifying assumption that the round trip cavity loss, t+L, is less than 25 percent. The parameter ℓ represents the active length, g_o, the small signal gain, t the transmission loss, L the distributed passive loss and A the cross-sectional area of the laser mode. The parameter I_s is the saturation at line center (v_o) and is given by

$$I_S(v_o) = \frac{hv_o}{\sigma_o(t_\mu + t_\ell)} \qquad (2-2)$$

where h is Plank's constant, σ_o is the cross section for stimulated emission, while t_μ and t_ℓ represent the lifetimes of the upper and lower lasing levels. These lifetimes can be decreased by molecule-molecule or electron-molecule collisions

in the gas volume, and by wall deactivation. However, at sufficiently high pressure, volume deactivation mechanisms dominate [> 60 Torr for a 2 mm sq. channel [21]] so that the $(t_{\mu}+t_{\ell})^{-1}$ term increases linearly with pressure. Since the cross section parameter σ_o also increases linearly with pressure in the homogeneously broadened regime, the saturation parameter $I_s(v_o)$ varies proportionally with the pressure squared [21, 22].

Returning to equation 2-1, it is evident that the gain and the distributed losses determine the output power of the laser. If the gain is much greater than the loss

$$2g_o\ell > t + L$$

Then

$$P_o \cong \frac{t}{t + L} I_s A g_o \ell \qquad (2\text{-}3)$$

which in the high pressure regime is proportional to the pressure squared.

On the other hand, the efficiency for extracting the power is given by

$$(1 - \frac{t + L}{2g_o\ell})$$

and depends upon the loss, gain fraction. Therefore, efficient operation can only be achieved when the small signal gain is large compared to the losses. Clearly an efficient high output power laser is only realized with a gas mixture which optimizes the loss gain fraction at a reasonably high gas pressure.

2.2 Importance of Cooling

The importance of cooling the CO_2 laser gas to obtain efficient laser operation is well known [62]. Increased cooling produces greater depopulation of the lower laser level which increases the gain and as was previously discussed, generates a higher output power. However, in waveguide lasers cooling is of even greater importance than it is in conventional D.C. excited carbon dioxide lasers because of the high thermal impedance of the small diameter waveguide structures [23]. Therefore, highly thermally conducting dielectrics such as BeO, BN and Al_2O_3 are often used, instead of glass, for the optical waveguide.

The effect of a high thermal impedance can be clearly demonstrated by considering a cylindrical bore waveguide containing a uniform heat source. A rectangular geometry would relate more closely to the transverse R.F. waveguide built (see Chapter 4) but the heat transfer equations are very complicated and can only be solved numerically. Therefore, the cylindrical geometry shown in Figure 2-1 is used to demonstrate the basic trends.

The conduction of heat from the gas through the tube wall can be predicted by applying Fourier's law [24].

$$q = -2\pi k_m \ell r \frac{dT}{dr} \tag{2-4}$$

Integrating and applying the appropriate boundary conditions generates an expression for the temperature gradient ΔT which develops across the wall of a hollow cylindrical discharge tube

$$\Delta T = \frac{q}{2\pi \ell k_\omega} \ln \frac{r_2}{r_1} \tag{2-5}$$

FIGURE 2-1

Geometry used for the Temperature Gradient Calculation.

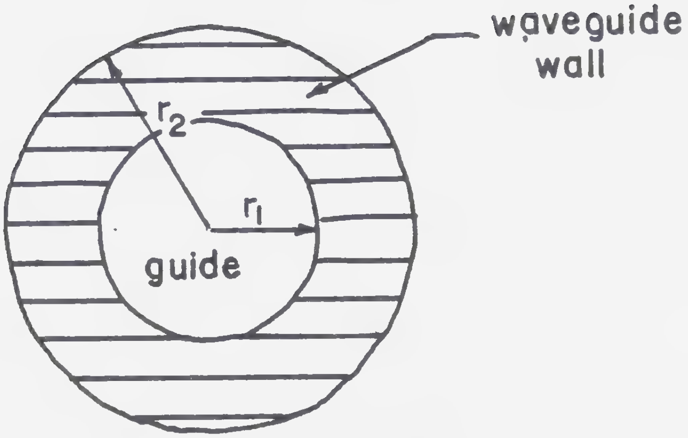

TABLE 2-1

Thermal Conductivity and Linear Thermal Expansion Coefficients of Four Potential Waveguide Materials

Material	Thermal Conductivity cal/cm sec°C at 20°C		Linear Expansion 10^{-6}/°C at 20°C		Reference
BeO (High Purity)	0.58		9.30		29
Al_2O_3 (99.5%)	0.069		8.60		30
BN[1] HBC grade	⊥ 0.05	II 0.08	⊥ 0.60	II 0.35	31
Fused Quartz	0.003		0.55		30

[1] ⊥ II indicates orientation of c axis to pressing direction.

TABLE 2-2

Calculated Temperature Gradient Across the Guide Wall For Four Potential Waveguide Materials With an Input Power Density of 3.3 Watts/cm and $r_2/r_1 = 5$

Guide Material	Gradient °C	
BeO	0.3	
Al_2O_3	2.5	
	⊥	II
BN	3.5	2.2
Fused Quartz	58	

The thermal conductivities for several potential waveguide materials are displayed in Table 2-1, while Table 2-2 compares some typical results using equation 2-5. Clearly BeO is potentially the best material while BN and Al_2O_3 are a close second. Fused quartz however, is a very poor choice.

2.3 Optical Losses

The output power of the laser, as was discussed in the first section, is maximized efficiently only when the distributed loss (L) within the guide is reduced. In a waveguide laser the distributed losses are generated by absorption within the guide, by scattering from the guide walls, by finite bends in the channel and by coupling losses at the mirror. Each effect produces a particular loss coefficient which when added together yield a net loss. For example, Papayoanou [27] describes the operation of a 12% efficient waveguide laser for which he estimates a total round trip cavity loss of 3 percent.

Since one of the consequences of reducing the dimensions of the laser to those of a waveguide is the introduction of losses due to the waveguiding action [1], the magnitude of this loss must be estimated. Equations 2-6 and 2-7, derived by Laakmann and Steier [28], can be used to predict the guiding losses of the lowest order EH mode in a rectangular guide. Two separate absorption coefficients arise because of optical polarization.

$$\alpha^x_{EH_{11}} = -\frac{1}{a}\left(\frac{\lambda}{4a}\right)^2 \mathrm{Re}\left[\frac{\varepsilon_a}{(\varepsilon_a - 1)^{\frac{1}{2}}}\right] - \frac{1}{b}\left(\frac{\lambda}{4b}\right)^2 \mathrm{Re}\left[\frac{1}{(\varepsilon_b - 1)^{\frac{1}{2}}}\right] \tag{2-6}$$

$$\alpha^y_{EH_{11}} = -\frac{1}{a}\left(\frac{\lambda}{4a}\right)^2 \mathrm{Re}\left[\frac{1}{(\varepsilon_a - 1)^{\frac{1}{2}}}\right] - \frac{1}{b}\left(\frac{\lambda}{4b}\right)^2 \mathrm{Re}\left[\frac{\varepsilon b}{(\varepsilon_b - 1)^{\frac{1}{2}}}\right] \tag{2-7}$$

The directions of x and y and the definitions of a and b are displayed in Figure 2-2.

Theoretical calculations were made for homogeneous and hybrid waveguides using the relative dielectric constants given in Table 2-3. The results of these calculations are displayed in Table 2-4. Clearly, the best guide material is BeO which yields a loss coefficient some two orders of magnitude lower than that for alumina and boron nitride. The hybrid structures displayed in the lower half of the table yield a factor of two improvement over their homogeneous counterparts. The type of metal, however, is not very significant since Ag, Au, Cu and Pd all yielded similar results. Clearly for the hybrid structures the preferred polarization corresponds to the smallest loss coefficient.

Scattering losses are difficult to predict without utilizing complicated probabilistic arguments. As a working criterion, to ensure minimum scatter, the surface should be polished so that all pits and scratches are less than 10 μm in size. However, the most important factor which reduces the scattering loss is the grazing angle reflection mechanism. In the literature only a single attempt has been made to assess the effect of scattering on the operation [36] of a waveguide laser. Abrams [36] observed a three percent loss when a CO_2 laser beam was reflected at grazing incidence, from a rough sandblasted piece of glass. However, when the glass was replaced with a polished surface the loss was effectively eliminated. Therefore, Abrams constructed a rectangular waveguide using four ceramic blocks which were polished prior to assembly. This method of assembly is also used by Laakmann Lasers Inc. [37], which polishes its waveguide surfaces to less than 10 microinches rms. [38].

Optical loss due to finite bends in a cylindrical hollow waveguide was first analyzed theoretically by Marcatili and Schmeltzer [1]. Garmire et al. [39]

FIGURE 2-2

Geometry of the Hollow Rectangular Dielectric Waveguide.

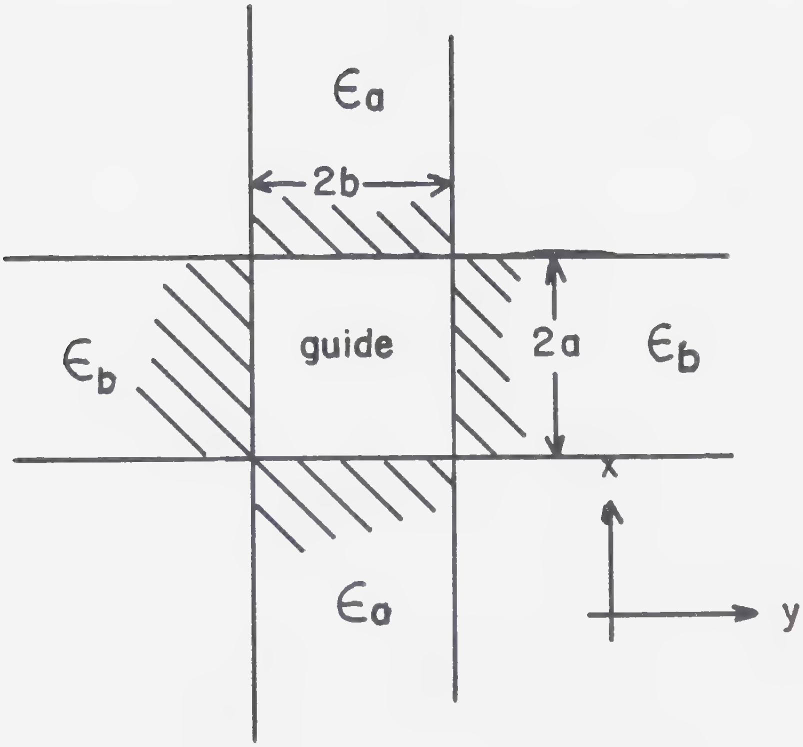

TABLE 2-3

Dielectric Constants Used to Evaluate Optical Transmission Losses.

Material	Dielectric Constant	Source
BeO	$\varepsilon = -2.25 + i.153$	32
BN	$\varepsilon = 16.25 - i1.82$	33
Al_2O_3	$\varepsilon = 1.32 - i0.033$	34
Ag	$\varepsilon = -2747 - i1404$	35

TABLE 2-4

Theoretical Absorption Losses for Several Homogeneous and Hybrid Hollow Waveguides

Configuration of Guide	Absorption (m^{-1}) 1.5 mm sq Guide		2.5 mm sq Guide	
	α^x	α^y	α^x	α^y
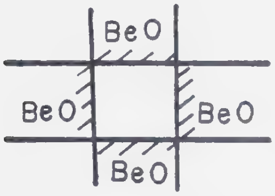	$1.15 \cdot 10^{-3}$	$1.15 \cdot 10^{-3}$	$2.48 \cdot 10^{-4}$	$2.48 \cdot 10^{-4}$
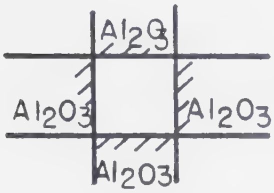	$6.79 \cdot 10^{-2}$	$6.79 \cdot 10^{-2}$	$1.46 \cdot 10^{-2}$	$1.46 \cdot 10^{-2}$
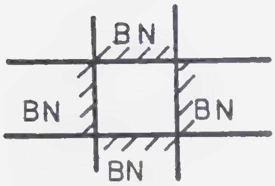	$3.76 \cdot 10^{-2}$	$3.76 \cdot 10^{-2}$	$8.11 \cdot 10^{-3}$	$8.11 \cdot 10^{-3}$
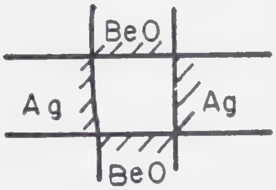	$1.0 \cdot 10^{-3}$	$2.17 \cdot 10^{-1}$	$2.16 \cdot 10^{-4}$	$8.36 \cdot 10^{-3}$
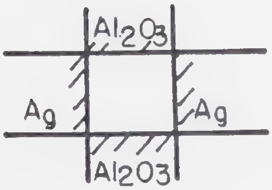	$3.87 \cdot 10^{-2}$	$2.46 \cdot 10^{-1}$	$8.35 \cdot 10^{-3}$	$5.3 \cdot 10^{-2}$
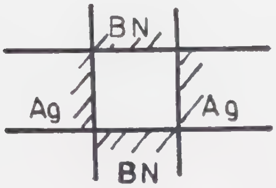	$3.55 \cdot 10^{-2}$	$2.19 \cdot 10^{-1}$	$7.66 \cdot 10^{-3}$	$4.71 \cdot 10^{-2}$

proposed that bending losses in a hybrid structure could be predicted using equation 2-8.

$$\alpha_b = \alpha_o \frac{\lambda^2}{2(2a)^3} \left(1 + \frac{21(2a)^6}{\lambda^4 R^3}\right) \tag{2-8}$$

where α_o is the loss calculated using equation 2-6 or 2-7, the dimension a and the radius R are defined in Figure 2-3. Using this relation some representative results are displayed in Table 2-5. To place the results in perspective consider that a 45 cm long laser can be machined such that the maximum surface variation from one end to the other will be no greater than two thousandths of an inch. This corresponds to a radius of 514 m, or an additional loss of only point one percent. Furthermore, experimental results [40] have demonstrated that these predictions are slightly overestimated.

Coupling losses are those losses which are incurred when the laser radiation leaves the guide and propagates to an external mirror which then images the beam back on itself into the guide. The losses arise because diffraction broadens the beam so that all the radiation is not returned to the guide. Three possible mirror configurations [41] can be used for waveguide lasers. Brewster angle windows are generally not used on high power cw waveguide lasers because of the high intracavity power densities which exist. The simplest method, for which no loss occurs, is realized by placing flat mirrors at the end of the guide. However, it is often more advantageous to place these flat mirrors a few millimeters from the end of the guide to permit gas flow. Also, the mirrors can then be mounted on an invar frame to enhance the thermal stability of the cavity. In such a situation, the loss incurred by placing a flat mirror a distance d from the

FIGURE 2-3

Geometry Used to Calculate the Optical Loss Which Arises from a Finite Bend in the Guide. Note that the Displayed Bend is Exaggerated For the Purpose of Illustration.

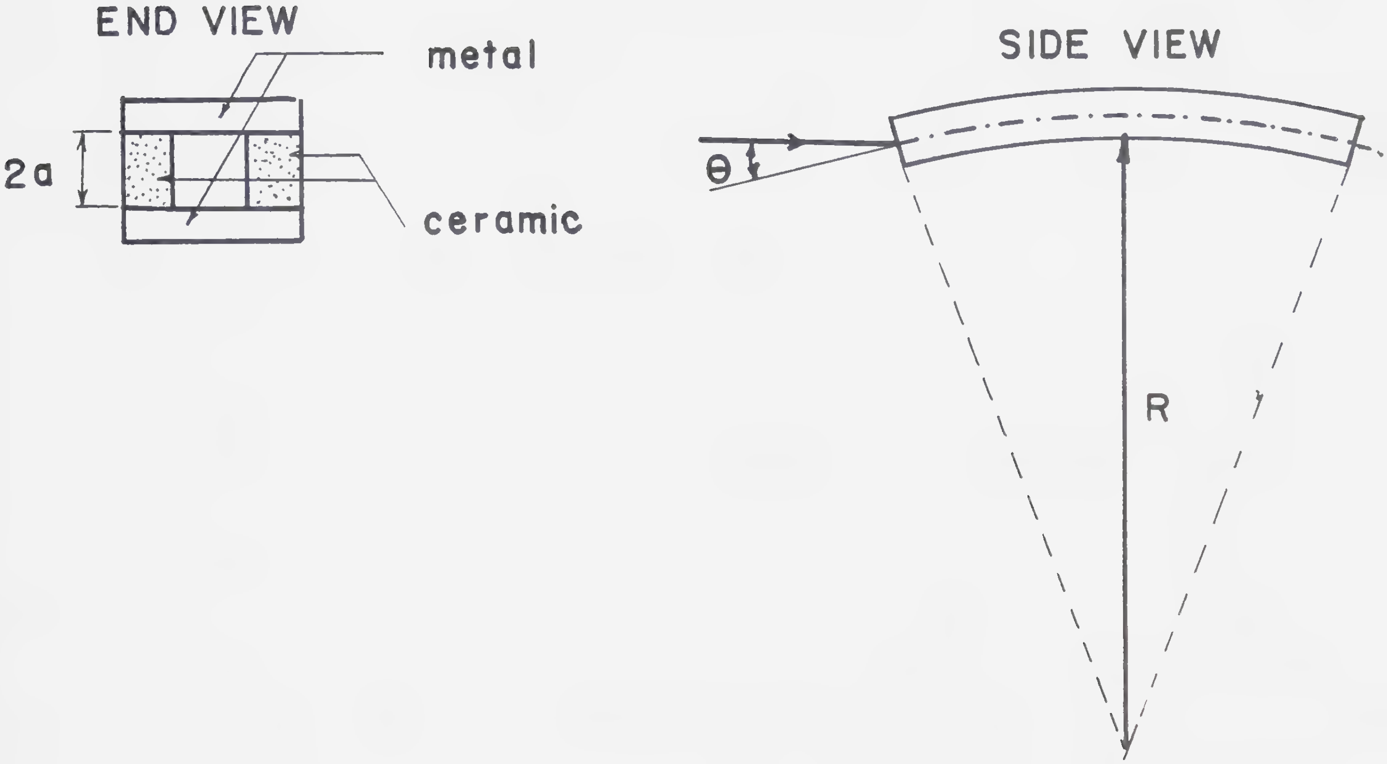

TABLE 2-5

Radius of Curvature of a Planar Guide for Which The Optical Absorption Loss Doubles.

Channel Size	Radius
2.5 x 2.5 mm	27 m
2.0 x 2.0 mm	19.4 m

guide can be predicted using equation 2-9 [70]

$$\% \text{ loss} = 605\left(\frac{d}{ka^2}\right)^{3/2} \tag{2-9}$$

This formula only strictly applies to cylindrical guides. However, it can still be used to estimate the loss when a rectangular guide is employed. For example, a flat mirror placed 2.0 mm from a 2.5 mm x 2.5 mm guide will only contribute about 0.3% to the total optical loss of the system.

2.4 Transverse Mode Discrimination and Stability

To align the optics the mirrors must be arranged parallel to each other and perpendicular to the axis of the guide. Garmire et al. [42] experimentally determined that the lowest order mode will be predominantly excited so long as

$$\Theta < \frac{\lambda}{4a}$$

where Θ, as shown in Figure 2-3, is identified by the intersection of the waveguide axis with a line segment drawn perpendicular to the laser mirror.

When the optics are properly aligned a single mode output is generated because higher optical losses are associated with the higher order modes. However, with bore sizes greater than 2.0 mm square, Hall et al. [43] report that the higher order modes cannot always be easily suppressed.

The laser output power stability is strongly controlled by thermal effects. Expansion and contraction of the reflectors and mirror mounts can alter the cavity length so as to shift the Fabry Perot resonance peak within the homogeneously broadened linewidth. This behavior produces output power fluctuations and forms a characteristic pattern known as the laser signature [44]. This power

variation can be suppressed by mounting the optics on an invar frame. Alternatively, the waveguide can be constructed from boron nitride with the optics fastened directly to the guide.

Instabilities can also be caused by thermally nonhomogeneous structures such as guides formed by clamping together strips of Al and Al_2O_3 [37]. In this case, as the laser warms up, the hybrid structure expands nonuniformly causing the guide to bend. As a result, the optical loss is increased and the mirrors are slightly misaligned so that a multimode output is generated. Fortunately, these undesirable effects can be substantially reduced by employing a homogeneous waveguide [37].

2.5 Power Supply Operating Frequency

The optimum R.F. operating frequency is very difficult to predict because of the large number of factors which affect its choice. Clearly, the best method would include a value chosen through experimentation. However, such a method requires an expensive broad band R.F. power supply. At the start of this work no such source was available so an alternate method was used to choose the optimum operating frequency.

The most important characteristic of a R.F. gas discharge is its positive impedance characteristic. Such a discharge is also characterized by a potential which, once breakdown is achieved, falls appreciably below its breakdown value due to the loading of the oscillator. This potential can be further reduced by decreasing the current until a minimum maintenance potential is reached. A further decrease in current will now cause the potential across the discharge to increase until it reaches the extinction potential, at which time the discharge will go out. This increase in voltage signals the transition from a positive impedance

regime to a negative impedance regime [9].

The running voltage in a R.F. discharge has also been shown to be frequency dependent [45, 15], declining slightly as the operating frequency increases. This effect has special implications for laser applications where the efficient excitation of the carbon dioxide gas molecules depends upon the magnitude of the applied field.

Examination of the literature [9] reveals that 4 different high frequency discharge regimes exist depending upon the discharge size, the gas pressure and the operating frequency. For RF excited carbon dioxide waveguide lasers a gas discharge dominated by ionization and diffusion without secondary processes is desired. Griffith [47] has calculated that for a 1.5 mm square bore channel the operating frequency must be greater than 13 MHz. In his analysis, Griffith reasoned that during the time the applied field is orientated in a single direction the electrons and ions must not be able to drift from one electrode to the other. Such a drift, if permitted, would contribute to secondary losses and support discharge instabilities.

Experimentally, Laakmann [15] demonstrated that a stable carbon dioxide gas discharge in a 2.0 mm sq bore metal-ceramic guide cannot be realized with a source frequency less than about 30 MHz. However, Lachambre et al. [48], using an all ceramic guide, produced a stable CO_2 gas discharge at 21 MHz. Although these results are somewhat inconclusive, they do indicate that a low frequency limit exists in the range of 10 to 30 MHz.

Of equal importance is the high frequency limit. As was discussed, the operating voltage decreases as the source frequency is increased. This effect is desirable for efficient laser operation. However, as the operating frequency increases the R.F. propagation velocity in the waveguide decreases generating a

voltage variation along the electrode. Clearly voltage variations are undesirable for efficient gas excitation. Researchers at United Technologies [49] have indicated that at 150 MHz such variations arise while workers at Hughes Aircraft Co. indicate that standing voltages are not a problem at 150 MHz [50].

Workers at Hughes Aircraft [50] also observed that the operating frequency range without voltage variations could be greatly increased by making the side walls as thin as possible. To understand why this improves the waveguide behavior the laser discharge must be modeled as a lossy microstripline. Figure 2-4 indicates that the model is reasonably accurate although the laser structure is certainly nonhomogeneous.

A microstripline is not an ordinary transmission line since its structure gives rise to complex fringing patterns of the electric field lines. In turn, this pattern results in an effective value of the dielectric constant which is lower than would be measured by incorporating the ceramic material within a capacitor structure. In the stripline structure, as shown in Figure 2-4, the ratio w/h exerts a strong influence upon the effective value of the relative dielectric constant [51]. For example, with an alumina substrate and a w/h of 100 the effective relative dielectric constant is 9.8. However, if the ratio is reduced to 0.1 the effective relative dielectric constant drops to 6.0. Therefore, by reducing the electrode width and the side wall thickness, the relative dielectric constant is reduced. In turn, the source wavelength is increased which ultimately leads to increased R.F. propagation velocities and decreased voltage variation along the electrodes. Examination of the data in Table 2-6 reveals that, to reduce the effect of voltage variations, BN would be the best candidate for a waveguide material. Therefore, the maximum operating frequency depends upon the material used to construct the waveguide.

FIGURE 2-4

Comparison of the Waveguide Laser Geometry and A Microstripline Cross-section.

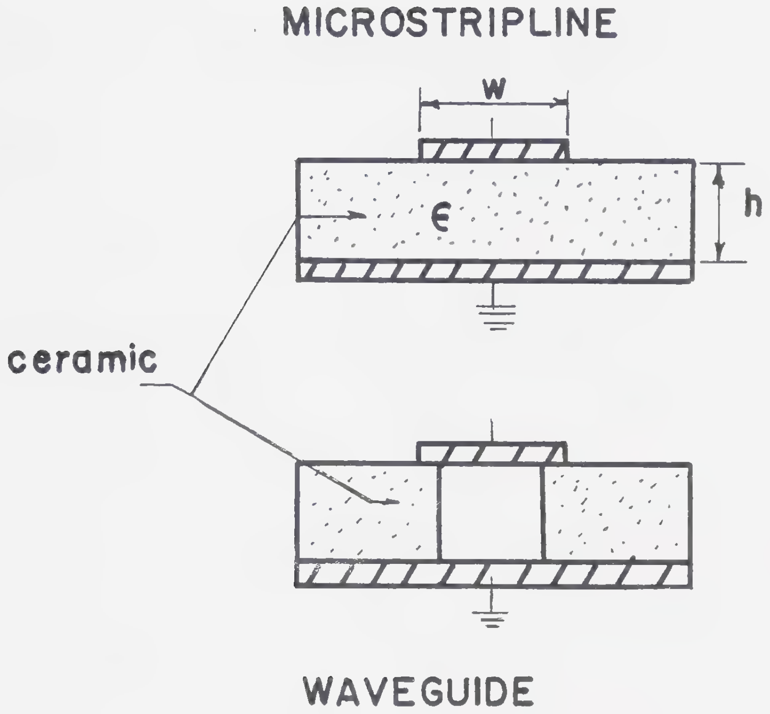

TABLE 2-6

Electrical Properties of Three Potential Waveguide Materials[1].

Material	Dielectric Constant	RF Wavelength in Ceramic	Loss Tangent $\times 10^{-4}$	Reference
BeO	6.7	1.16 m	1.0	29
Al_2O_3	9.3	0.98 m	0.6	30
BN	4.6	1.40 m	1.5	31

[1] All values measured at 100 MHz.

2.6 Design Criteria

As has been discussed, an efficient waveguide carbon dioxide laser operates best when the passive cavity losses are minimized and the gas temperature is reduced to the lowest practical value. With these requirements in mind 4 possible materials, beryllium oxide (BeO), aluminum oxide (Al_2O_3), boron nitride (BN) and fused quartz (glass) were considered as potential guide materials. Fused quartz was eliminated because it is a very poor thermal conductor. Beryllium is optically and thermally the best choice, but because of fabrication difficulties associated with the toxicity of airborne BeO dust it was also rejected.

Boron nitride offers the lowest relative dielectric constant and excellent thermal stability, but it is extremely difficult to metallize. Therefore, BN was not employed. Alumina was chosen because its thermal and optical properties are acceptable. The material could be ground and cut with equipment available at the University and metallization was simplified by the low processing temperature ($850^{\circ}C$) metal thick film compounds which are commercially available [52].

To design a waveguide laser the input power per centimeter is an important characteristic. The R.F. supply which was used in this development program included four separate amplifiers, each producing 100 watts of power. Therefore, the discharge length into which 100 watts of power was to be matched had to be estimated. Table 2-7 was consulted, then 0.3 watts of laser power per centimeter at 10% efficiency were adopted as design specifications. This choice implied that a minimum of 100 watts of R.F. power had to be deposited into a 30 cm length of channel.

As theoretical calculations have shown, the optics had to be mounted within 2 mm of the channel so that coupling losses would be minimized. ZnSe

TABLE 2-7

High Power CW CO_2 Waveguide Lasers Reported in the Literature Prior to July 1982.

Laser (Author)	Efficiency	Laser Power (Watts)	Power/cm (Watts/cm)	Reference
Laakmann	10%	30	0.3	65
Carter & Marcus	--	39.5	0.51	67
Papayoanou	12%	9	0.36	27
United Technologies	15% 10-15%	22.5 38.0	0.66 0.52	49

Note: Abrams and Bridges [22] estimate that the maximum available output power/unit length in a waveguide laser, neglecting all losses, is 0.9 watts/cm.

output couplers were chosen because of the ability of these optics to withstand the high intracavity power densities which exist in waveguide lasers. The optics were ¼ inch diameter and were supported in metal mounts which also acted as heat sinks. The reflectivity of the output coupler could not be chosen in advance because the cavity losses were not known. As is well known, the optimum output coupling (for maximum power) increases as the cavity losses increase. Therefore, a variety of different output coupling mirrors (90, 80, 85, 75% R, etc.) were purchased so that this operating parameter could be optimized.

The R.F. power supply was chosen to operate at 72 MHz. This value was chosen well above the minimum of 30 MHz, but was not too high so that the effect of a standing voltage could be reduced.

With these choices made in advance, further research was conducted to assess the standing voltage problem, impedance matching networks, channel size and fabrication techniques. These experiments are discussed in greater detail in Chapters 3, 4 and 5 of this report.

CHAPTER 3

RADIO FREQUENCY GAS DISCHARGE EXPERIMENTS

3.1 Construction of the Discharge Structure

The R.F. discharge experiments were performed to investigate the potential impedance matching networks, transmission line effects and to ensure that the solid state R.F. power supply was able to maintain a uniform discharge at gas pressures of 30 to 200 Torr for a variety of waveguide channel sizes.

The basic discharge structure, shown in Figure 3-1, included a square bore, 30 cm long, with a transverse electrode configuration. The channel was formed by grinding a groove in an alumina block using a diamond grinder. This block was epoxied to the water cooled Al ground plane. The top electrode was held in place by teflon clamps. Clamping techniques are also used by Hughes Aircraft [53] and Laakmann Electro-optics [54] to produce hybrid waveguides. The entire structure was surrounded by a transparent vacuum envelope.

Connected to the discharge structure, see Figure 3-2, via an impedance matching network was a bidirectional power meter capable of measuring 250 watts of forward or reflected power and a 100 watt R.F. power supply. The matching network was used to transform the complex load impedance so that it matched the 50 Ω co-axial line impedance. The electrical feedthrough was connected to the center of the upper electrode so as to reduce transmission line effects. Initially a 1.6 mm square bore channel was used with a lean gas mix (16:2:1, $He:N_2:CO_2$). This gas mixture was available in a premix form, therefore it was often used. In the remainder of this report this mixture will be referred to as premix while other gas mixtures will be specifically described.

FIGURE 3-1

Transverse and Longitudinal View
of the Gas Discharge Structure

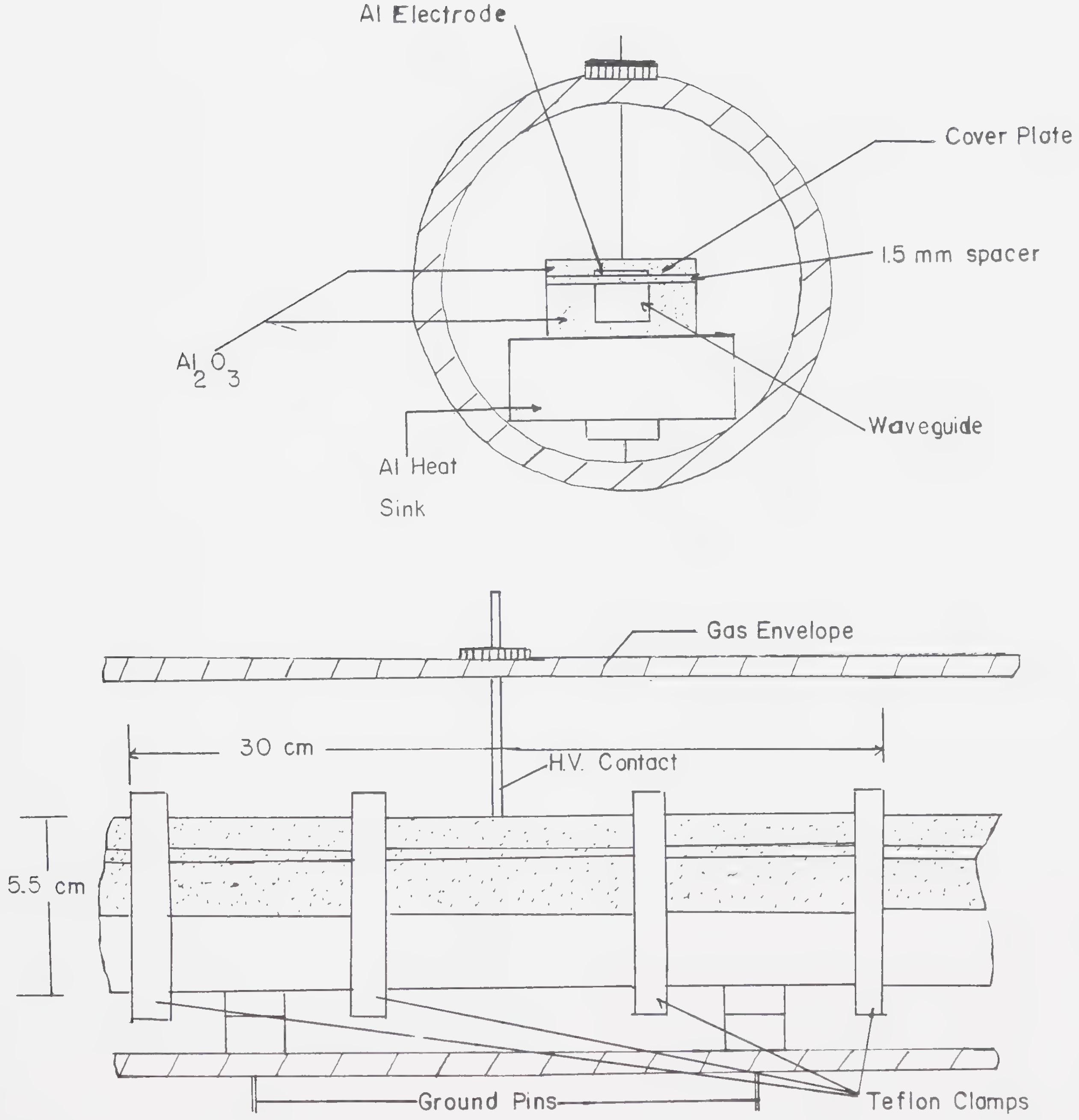

FIGURE 3-2

Schematic of the Experimental Discharge Apparatus

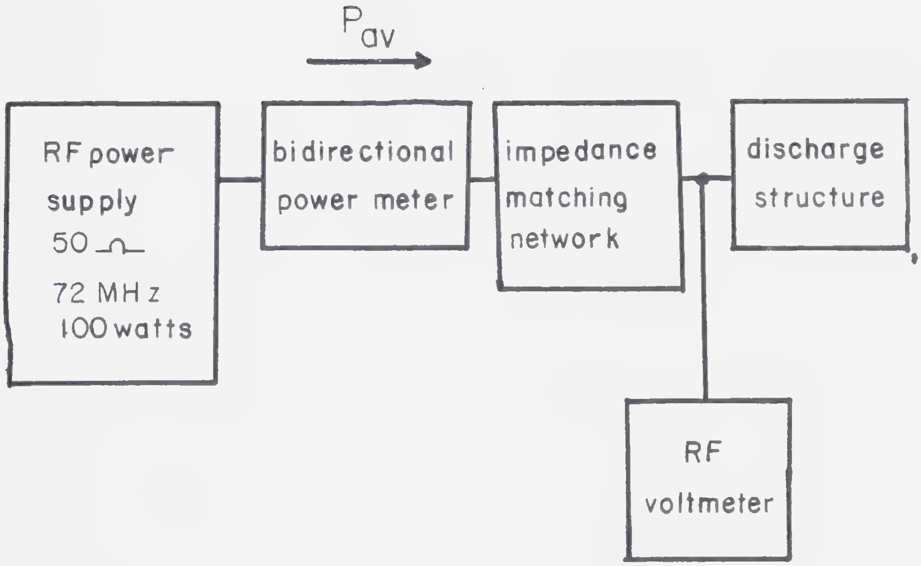

3.2 Experiments

The first set of discharge tests assessed the various matching schemes. The discharge structure was modeled as a capacitor in parallel with a resistor. The capacitance was measured to be 30 pF, while the resistance depended on the gas mixture, operating pressure and input power. All three networks, shown in Figure 3-3, contain capacitances which are less than 150 pF and inductors ranging from 0.2 to 0.4 μH. As shown in Figure 3-3, networks 2 and 3 performed best, but the third network was used in subsequent tests because it could be tuned most easily. Using this network and a 1.6 mm sq bore channel, uniform discharges at pressures ranging from 20 to greater than 200 Torr were realized.

Previous analysis (see Chapter 2) indicates that if this channel were used as a laser it would exhibit about a 7% loss for a one meter length. This loss is excessive, therefore the channel was enlarged to 2.5 mm sq which reduced the loss to less than 2% for a one meter path length. As a result of this change the channel capacitance rose to 36 pF which correspondingly drove the Q of the matching circuit higher. Subsequently, the impedance match was more difficult to obtain and maintain while the electrical noise production rose. A further increase of the discharge structure capacitance to 46 pF worsened this situation.

The capacitance must also be maintained at a low value to reduce R.F. losses [53]. Alcock and Hall [55] performed a simple analysis in which the laser head was modeled as a capacitor C in parallel with a resistor R_D. They showed that the ratio of power P_D dissipated in the discharge, to the total power P_T delivered is given by

$$\frac{P_D}{P_T} = \frac{1}{1 + \frac{R_S}{R_D}\left(1 + \omega^2 C^2 R_D^2\right)}$$

FIGURE 3-3

Some Typical Matching Networks Used to Transform the Laser Head to a 50 Ω Equivalent
(All R.F. Powers are Expressed in Watts)

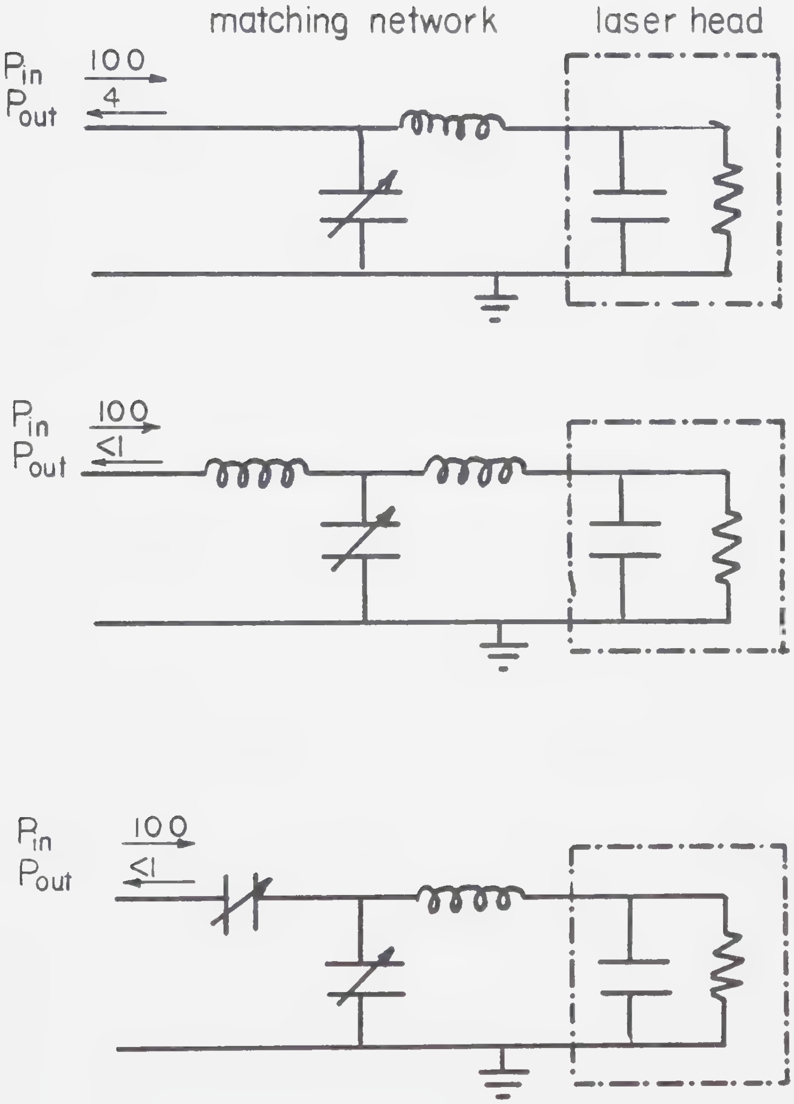

where w is the angular frequency and R_S is the ohmic resistance of the matching network which is effectively in series with the discharge. In principle, the channel capacitance and the series resistance must be maintained as low as possible to efficiently transfer the R.F. power into the discharge. For example, let $R_S = 0.5\ \Omega$, $R_D = 1\ k_\Omega$, C = 30 pf and f = 72 MHz. Then only 52% of the total input power reaches the discharge.

The example cited above indicates that a considerable quantity of power can be lost in the matching network. This result was experimentally confirmed by the resonating inductor which became extremely hot after only a few minutes of operation. Attempts were made to reduce this loss. Initially #18 gauge wire was used, but it was soon replaced by #16, then #12 and finally #8 gauge wire. However, no significant improvement was noted.

These early discharge experiments were also hampered by unreliable amplifier behavior. The amplifiers were found to quickly overheat so that a constant reliable power level was not available. In addition, repeated reflections of R.F. power degraded the performance of the amplifier.

To eliminate the heat problem the amplifier case was opened and air was forced across the printed circuit board as well as the heat sink. The improvement, documented in Figure 3-4, occurred because of the lossy nature of the output capacitors.

Transistor failure was attributed to the severe mismatch which takes place while the matching network is adjusted. Although the transistors could survive open and short circuits a partial mismatch generated destructive parasitic oscillations. Experimentation revealed that a mismatch of greater than 20% was sufficient to produce these parasitic oscillations. The R.F. transistor is actually composed of a large number of smaller transistors. The parasitic oscillations

FIGURE 3-4

Curves to Demonstrate the Effect of Forced Air Cooling. Curve c Represents Cooling by Natural Convection, Curve b Represents Forced Air Cooling of the Heat Sink, While Curve a Displays the Effects of Air Cooling On Both Sides of the Circuit Board.

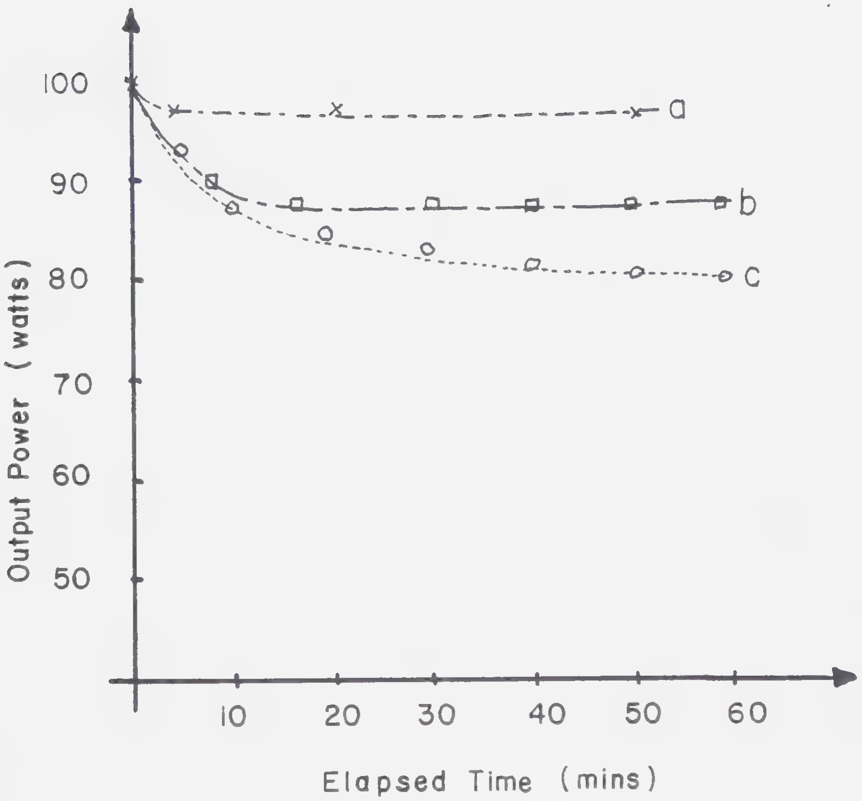

slowly destroyed these component transistors to produce an observable power drop. Since impedance mismatches were unavoidable the transistors were replaced when the amplifier output power declined to less than 75 watts.

In an effort to eliminate the problems associated with the channel capacitance a different matching technique was employed. The channel capacitance was resonated at 72 MHz with a parallel inductor [49, 46]. Heath kit dip meter was employed to insure that the resonance was tuned to 72 MHz. Therefore, at the operating frequency, the channel appeared as a pure resistance. The loss of capacitance lowered the resonant currents in the external matching network causing a substantial drop in the "Q" of the circuit. Also, with this matching technique the effective R.F. power transfer is no longer influenced by the channel capacitance because only the resistive component of the discharge affects the resonant currents in the external matching network.

The discharge structure now included a single, parallel inductor connected across the center of the structure. With this arrangement discharges up to 80 torr were realized. At higher pressures gaps began to form in the discharge. Initially these gaps were believed to be caused by the inability of the matching network to provide an adequate voltage step-up. However, when the 1.5 mm ceramic spacer was removed the measured voltage across the discharge dropped from 305 to 265 volts but the discharge behavior remained unchanged. These gaps, therefore were attributed to voltage variations along the electrode.

3.3 Modeling the Discharge

To verify that these voltage variations did exist the discharge was modeled using a solid resistive material to represent the discharge [49]. A low

power tunable R.F. oscillator was used to study the effects of a variety of parameters on the standing voltages.

The effect of the power supply frequency on the magnitude of the voltage variation is shown in Table 3-1. As was expected the lower the frequency the smaller the standing voltage variation. The actual profile is shown in Figure 3-5.

Next, the power supply was set at 72 MHz and the importance of multiple inductors was examined. The results in Table 3-2 indicate that the voltage variation is reduced by increasing the number of inductors [46]. The profiles for three cases are shown in Figure 3-6. The effect of electrode length is shown in Table 3-3. As expected, the variation was reduced by shortening the electrode.

These experiments indicate that transmission line effects are very important in these devices. Therefore, the laser must be modeled not as a resistor and capacitor but rather, as a lossy transmission line.

3.4 Hybrid Discharge Structure

Employing the information gathered to this point a new discharge structure was constructed. This structure, as shown in Figure 3-7, was similar to that used previously except the homogeneous channel was replaced by a hybrid design. All the pieces were held in place by teflon clamps. The channel was 2.5 mm square bore, 30 cm long with three inductors spaced equally along its length. For impedance matching a π network was employed since it is easier to tune than a "T" network. The network in Figure 3-3c was no longer useful because the transformation from the 50 Ω cable was now made to an impedance greater than 50 ohms rather than less than 50 ohms [56].

TABLE 3-1

Variation of the Magnitude of the Standing Voltage as the R.F. Source Frequency is Increased

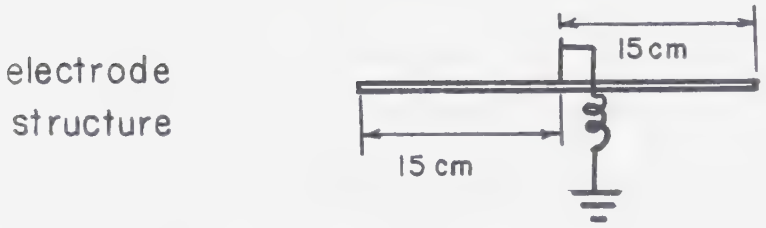

Power Supply Frequency (MHz)	Maximum Voltage Variation (as a percentage)
38	6%
53	9.4%
73	15.6%
109	22%

FIGURE 3-5

The Voltage Profiles Display the Effect of Reducing the R.F. Source Frequency. As the Frequency was Reduced From 109 (▫) Through 73 (▵) and 53 (X) to 38 (O) MHz, the Standing Voltage Also Declined. The Arrow Indicates the Position Where the R.F. Supply was Connected to the Electrode.

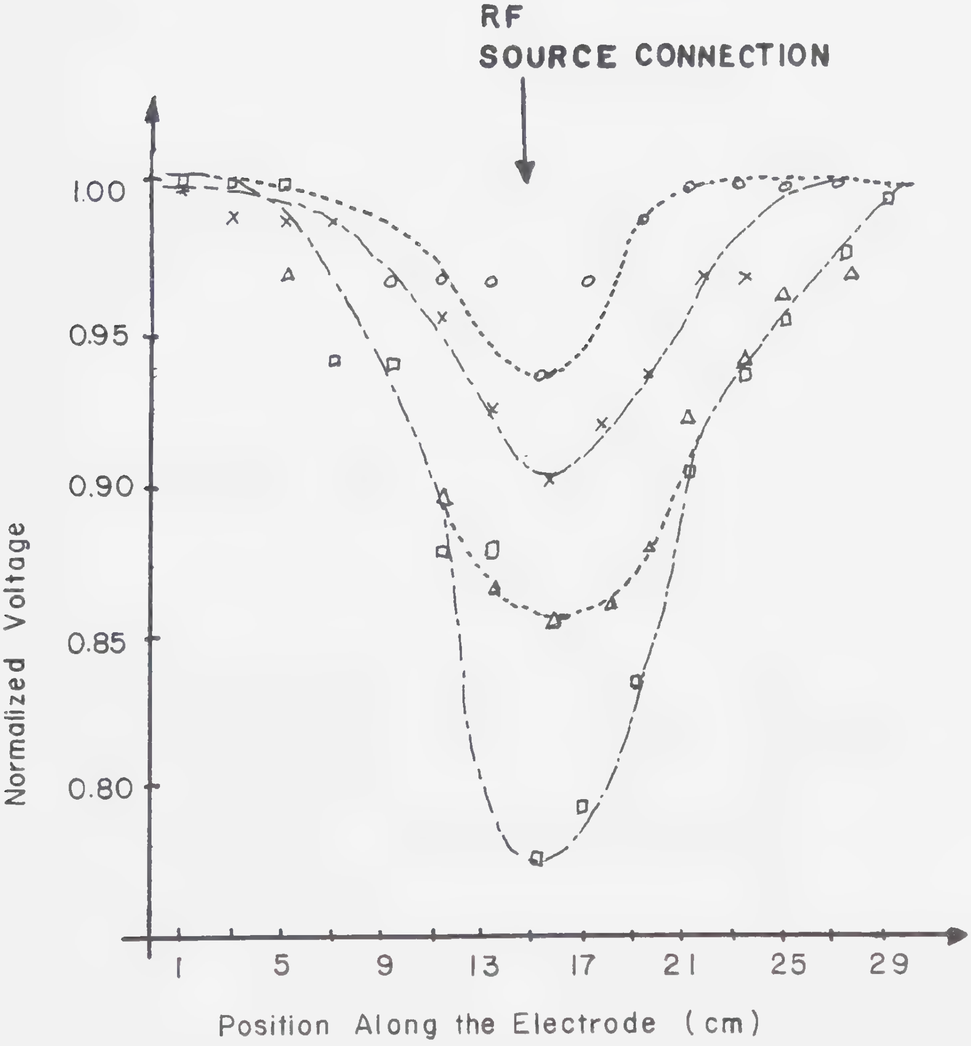

TABLE 3-2

The Variation of the Magnitude of the Standing Voltage as the Number of Resonating Inductors is Increased. A Source Frequency of 72 MHz was Used.

Configuration	Maximum Voltage Variation (as a percentage)
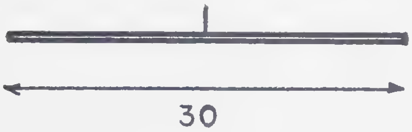	10%
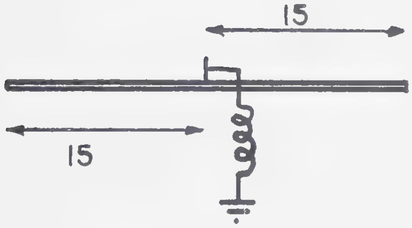	15.6%
	10%
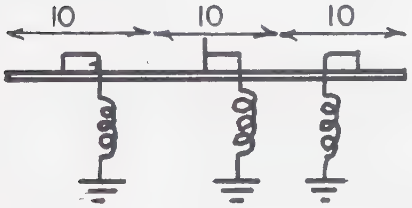	5%
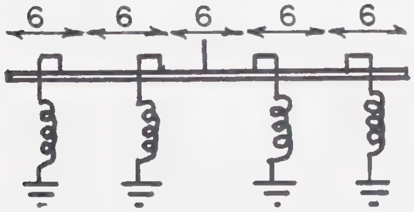	3%

FIGURE 3-6

As the Number of Inductors Positioned Along the Electrode Increased, the Maximum Voltage Variation Declined. The Figure Below Displays the Voltage Profile for Three (▫), Two (X) and Zero (0) Resonating Inductors. The Arrows Indicate Where the Inductors were Connected.

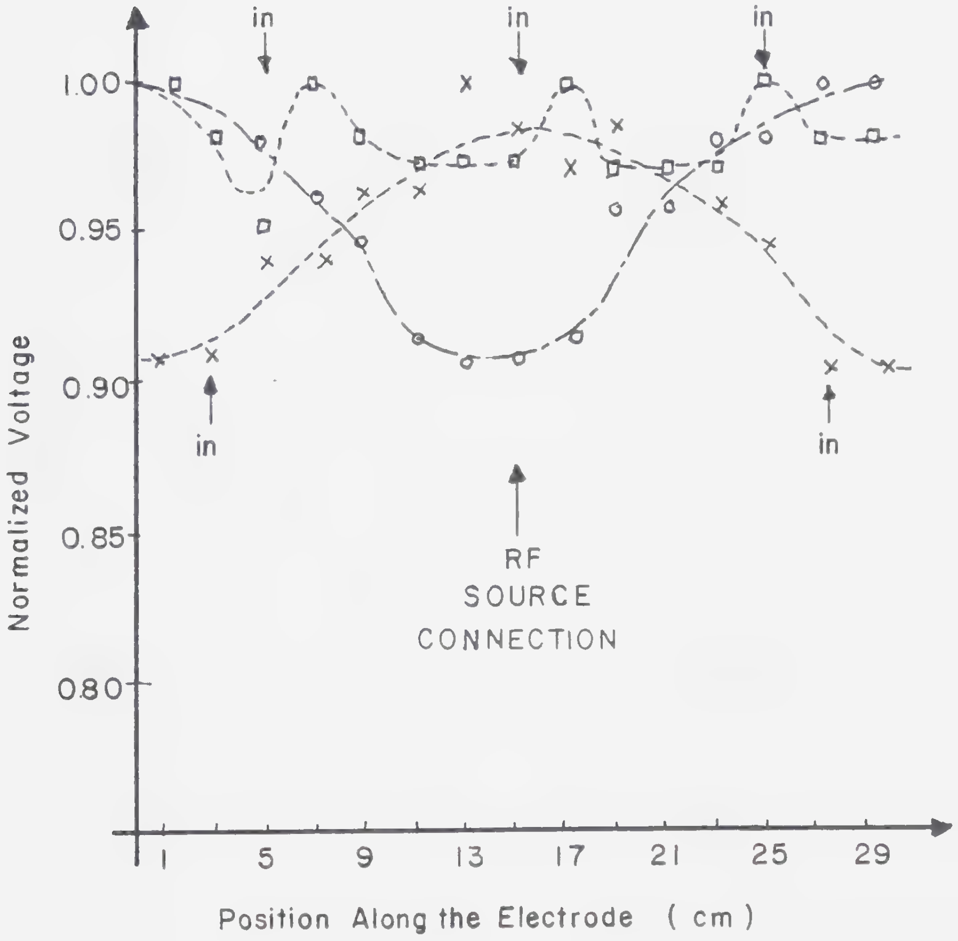

TABLE 3-3
The Variation of the Magnitude of the Standing Voltage as the Electrode is Shortened. A Source Frequency of 72 MHz was Used.

Configuration	Maximum Voltage Variation 30 cm Electrode	 15 cm Electrode
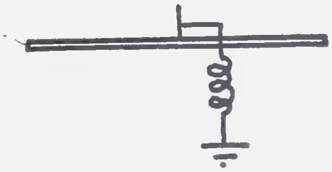	15.6%	6%
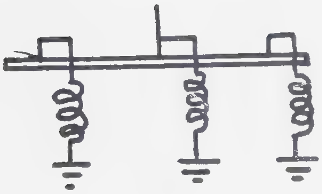	5%	3%

In addition to a more uniform voltage, this structure offered the further advantage of running at a lower voltage because two series capacitors were eliminated when the upper and lower alumina layers were replaced by aluminum electrodes. Also, the hybrid structure offered a factor of two improvement in optical loss, an important parameter when considering laser operation.

Using this structure, a uniform discharge was maintained in the premix gas at pressures up to 200 Torr. This result represented a considerable improvement. The upper pressure limit was now the result of the inability of the matching network to supply a voltage large enough to produce gas breakdown.

Using the experimental arrangement just described, the discharge voltage as a function of gas pressure was measured for three different gas mixtures. The corresponding field/pressure values were also calculated and are displayed in Figure 3-8. As a result of the invariance of the voltage from 60 to 100 Torr a wide range of field/pressure values were obtained. At higher pressures this ratio declined to less than 5 V/cm-Torr which is quite low and suggests that efficient laser operation should be obtained if the optical losses are minimized. For example, J. Lowke et al. [57] predicted that an E/P value of 7.5 V/cm-Torr for a 1:2:3 (CO_2:N_2:He) gas mixture is the optimum value for efficient gas excitation while a more lean mix favors a lower field/pressure ratio such as 3.5 V/cm-Torr for a 4:1:12 (CO_2:N_2:He) gas mixture.

To obtain further insight into the behavior of R.F. discharges, the voltage versus power characteristic of a 2 mm sq. bore by 30 cm discharge was measured. Figure 3-9 displays this curve at various pressures. Note that as the input power is reduced the positive impedance character is lost.

As this character declines the discharge begins to fade and finally is extinguished (arrow). This minimum power density, which increases with gas

FIGURE 3-7

Cross-Sectional View of the Hybrid Discharge Structure

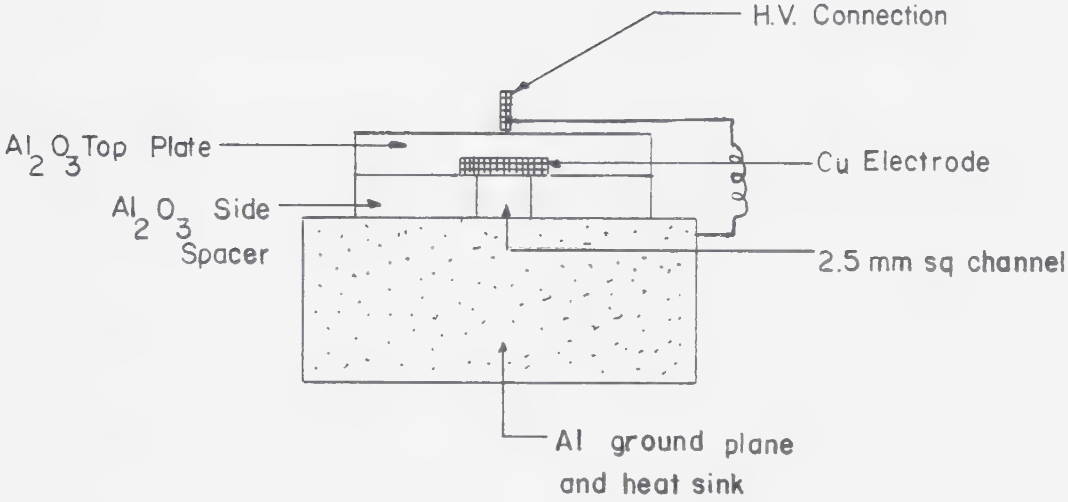

FIGURE 3-8

Variation of Voltage [---] and Field Pressure (E/P) Ratio [–] with Pressure for Different He:N_2:CO_2:Xe Gas Mixtures; X: [16:2:1:0]; O: [4.6:1:1:0]; △: [6.3:1.4:1.4:1]

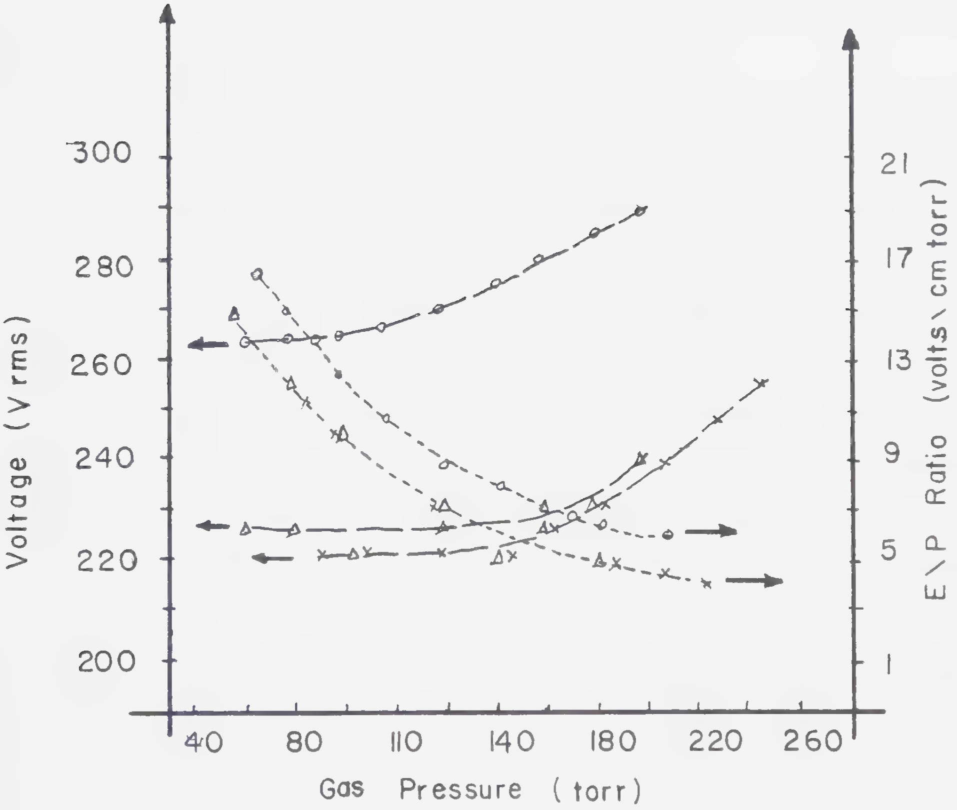

pressure, determines the maximum operating pressure. The maximum operating pressure also declines as a richer gas mixture is used. Furthermore, increasing the channel size reduces the input power density which, in turn, lowers the maximum operating pressure. Therefore, to increase the maximum operating pressure the input power density must be increased either by increasing the input power or reducing the discharge volume. The effect of channel size was examined further by running a 2.7 mm sq. x 30 cm discharge and a 2.0 mm sq x 30 cm discharge. Figure 3-10 demonstrates that the discharge voltage is a function of the input power density, not the electrode separation.

Although 72 MHz was chosen as the operating frequency, based upon the reasoning outlined in Chapter 2, two other sources, one operating at 40 MHz and the other a variable source at 30, 21 and 14 MHz, were obtained so that the effect of operating frequency could be analyzed. Using a metal ceramic sandwich structure with a 2.7 mm sq bore the voltage versus power density characteristic (see Figure 3-11) was obtained at 72 MHz, 40 MHz, 30 MHz and 21 MHz. The discharge became unstable for frequencies less than 30 MHz.

The instability occurred because the polarity of the alternating electric field, between the electrodes, did not reverse rapidly enough to prevent the electrons from drifting across the entire discharge [47]. Therefore, as the operating frequency dropped the drift losses increased until the discharge became unstable.

At the lower frequencies, however, the discharge stability was improved by separating the electrodes from the channel with ceramic spacers. The capacitive ballasting effect has been used for some time to stabilize pulsed lasers [58, 59] to produce uniform preionization of high pressure discharges [11, 60] and to control large volume CW discharges [61]. More recently dielectrics have been

FIGURE 3-9

The Variation of Discharge Voltage with Current For a Variety of Gas Pressures. The Premix Gas was Used With a 2 mm sq. by 30 cm Long Discharge Channel. The Arrows Indicate Where the Discharge Extinguished Itself.

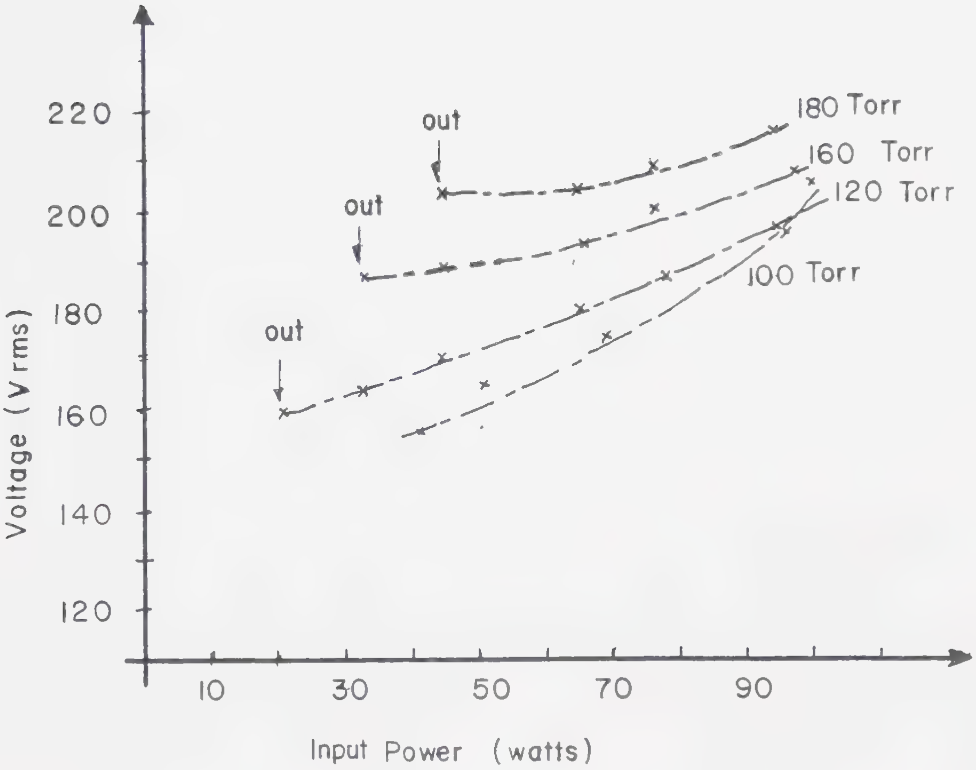

FIGURE 3-10

Variation of Discharge Voltage with Input Power Density. Two Channel Sizes 2.0 mm sq. [Δ] and 2.7 mm sq. [X] are Considered.

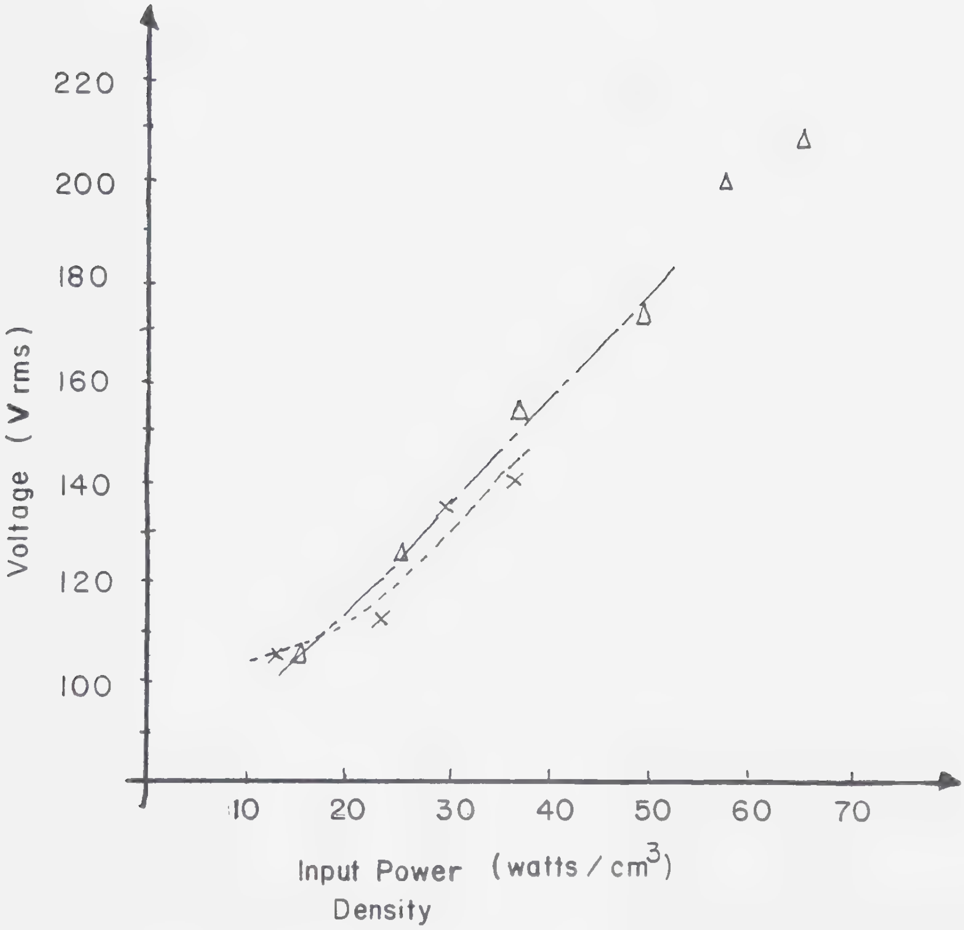

FIGURE 3-11

The Discharge Voltage Versus Input Power Density, Using a Variety of R.F. Supply Frequencies, is Displayed.
X: 21 MHz; △: 29.5 MHz; □: 40 MHz; O: 72 MHz.
The Arrows Indicate Where the Discharge Began to Contract or Disappear

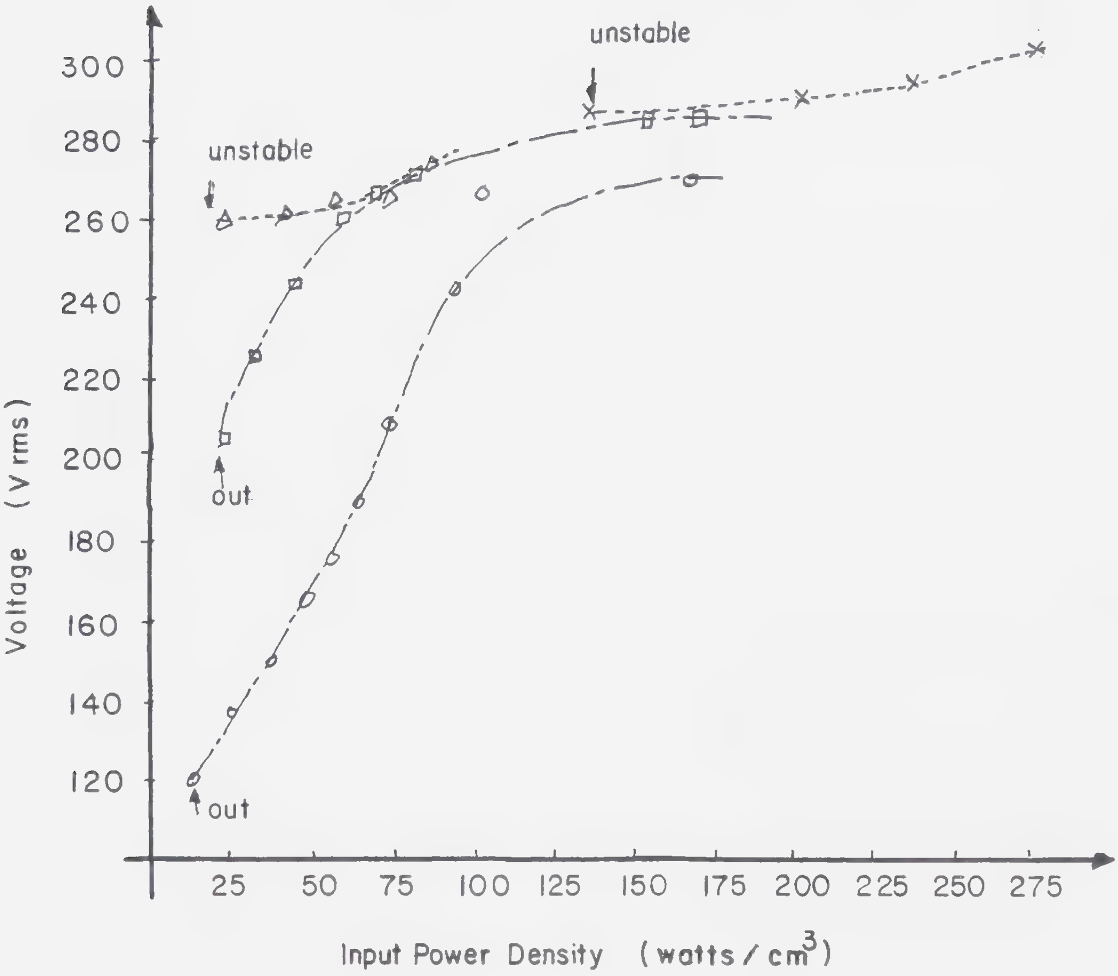

employed to stabilize pulsed [25] and CW R.F. excited carbon dioxide waveguide lasers [48].

The improved homogeneity associated with this discharge configuration can be traced to periodic charge accumulation on the dielectric surfaces. Space charge fields arising from charge buildup oppose the applied electric field serving as a negative feedback mechanism. This charge promotes uniformity of the R.F. current distribution over the dielectric surfaces. This uniformity of current distribution is then extended through the bulk of the gas, provided that the separation between the sheets is small (1-3 mm) [25].

At 30 MHz an alumina sheet 0.36 mm thick was found to provide sufficient ballasting so that uniform discharges were achieved in premix gas at pressures greater than 200 Torr. The channel was 2.7 mm sq by 30 cm long. This result was a considerable improvement over the 60 Torr maximum pressure that was realized with a metal ceramic discharge structure.

For an operating frequency of 21 MHz, the thickness of the ballasting plates had to be increased to greater than 1.8 mm before a stable discharge could be achieved to 150 Torr. Further increases in thickness failed to produce an improvement in the discharge stability because the R.F. supply and the matching network were no longer able to produce a voltage large enough to break down the gas. Obviously, as the frequency drops, the series voltage drop across the ballasting capacitance increases. This effect places a practical limitation upon the lower frequency limit.

Returning to Figure 3-11, a closer examination of the curves reveals that the discharge maintenance voltage declines as the source frequency increases [45, 46]. This behavior suggests that a more efficient field/pressure ratio may be achieved for a particular gas mixture by increasing or decreasing the R.F. source

frequency. Therefore, the ability to control the discharge voltage by changing the source frequency should enhance the efficiency of the carbon dioxide waveguide laser.

CHAPTER 4

THE 20 WATT WAVEGUIDE LASER

4.1 Construction Details

The design of the 20 watt waveguide laser evolved as the discharge experiments were conducted. The most important feature of this design was a hybrid metal-ceramic discharge structure resonated with three parallel inductors. The actual laser included two 30 cm sections clamped end to end, with each section driven by a 100 watt amplifier. The total system is shown in Figure 4-1a. Each external matching network was attached via a 12" 50 Ω coaxial cable to a bidirectional power meter which in turn was connected to a power amplifier. The π matching networks employed contained 150 pF variable capacitors with the inductor orientated far enough away from the capacitors to prevent field coupling. In this way input powers of 100 watts were achieved with less than 1 watt of R.F. power reflected.

The entire R.F. electrical system originated at a single oscillator which connected to a driver circuit. Beyond the driver a 4-way splitter network was employed so that 4 amplifiers could be driven.

Figure 4-1b displays the laser with the matching networks removed. The entire waveguide was surrounded by a transparent acrylic tube. The ZnSe optics were mounted on aluminum mounts, 2 mm from the guide; their orientation was adjustable using exterior controls. The laser radiation was coupled from the guide and propagated out of the gas envelope via a salt window which was attached to the end flange. The entire structure was "0" ring sealed except for the two electrical feedthroughs which were fastened in place using two swagelok fittings.

The waveguide structures is shown in Figure 4-2. The waveguide channel, which was 2.5 mm sq. and 60 cm long, was formed by clamping several

FIGURE 4-1a

The 20 Watt Waveguide Laser

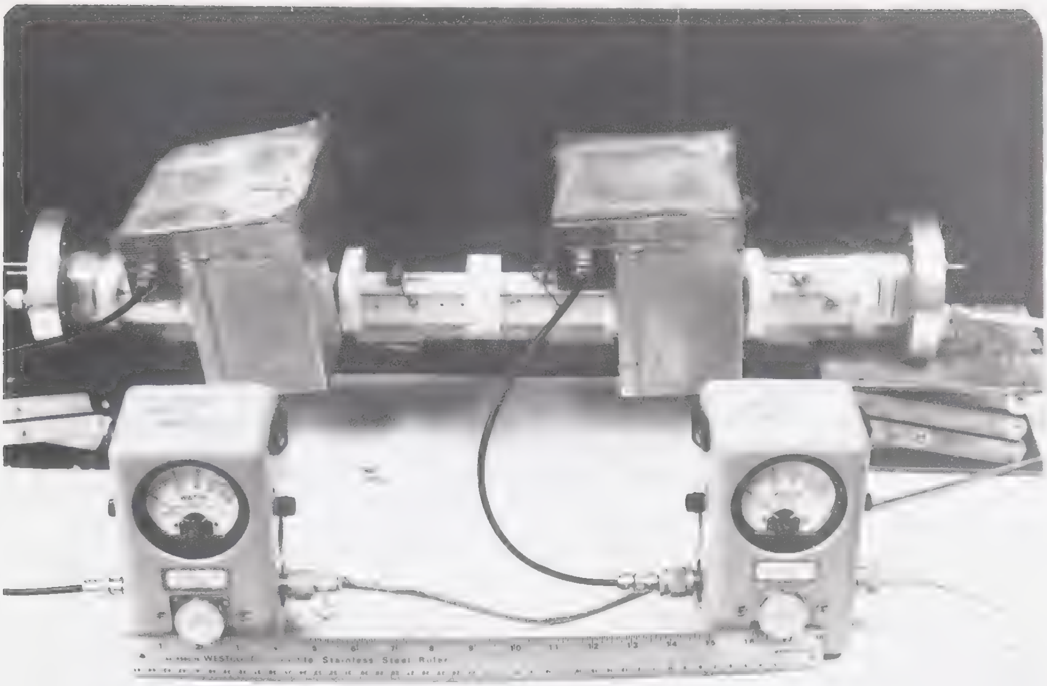

FIGURE 4-1b

The Waveguide Laser With Matching Networks Removed

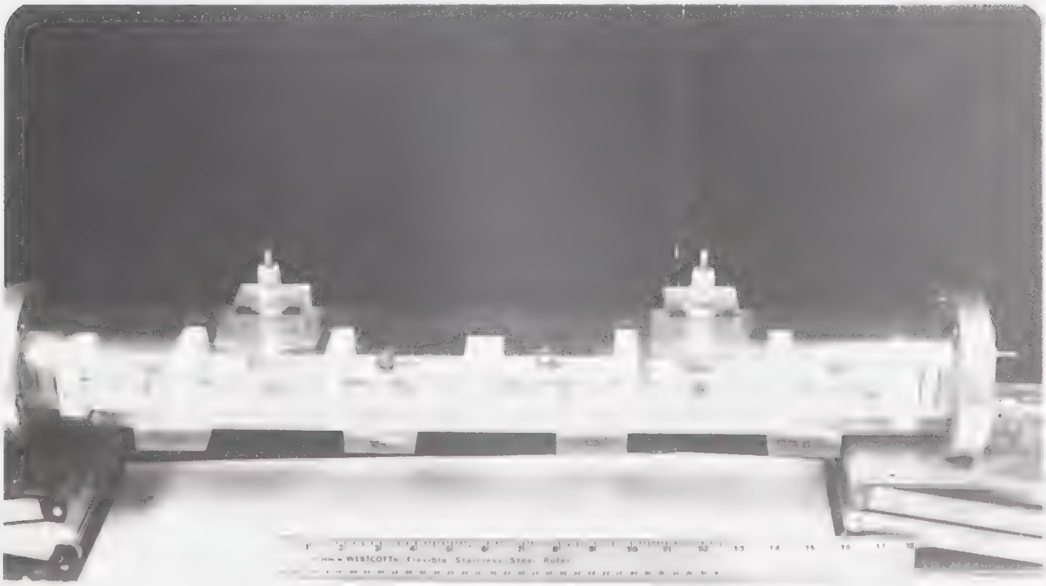

FIGURE 4-2

A Section of the Waveguide Laser
With the Top Plate and One Side Panel Removed

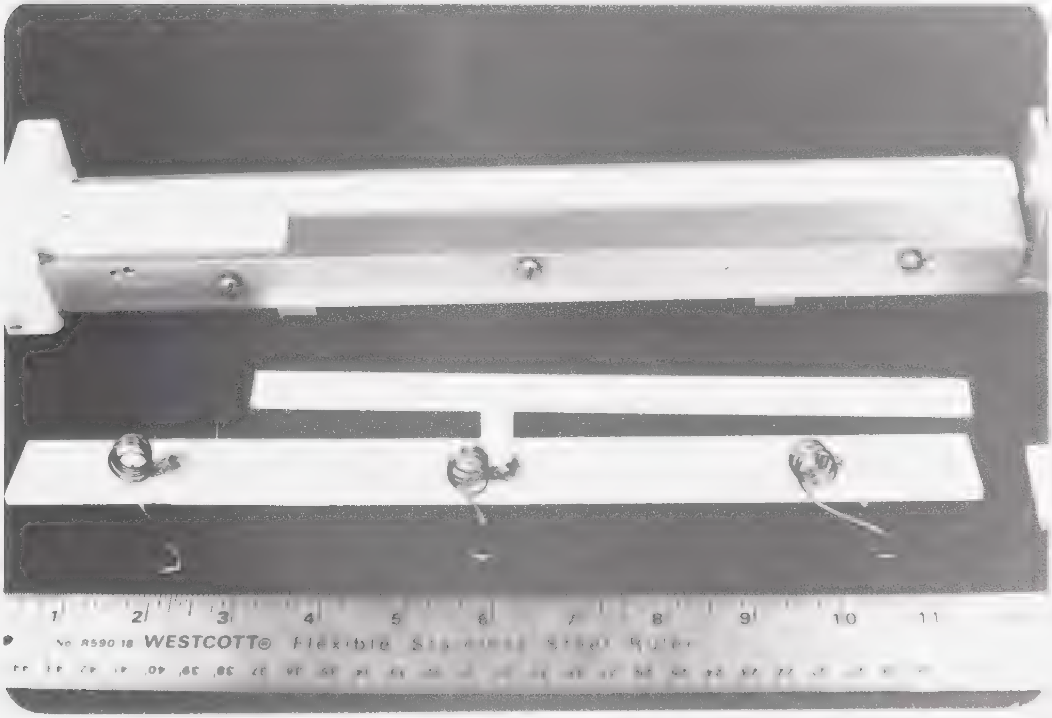

ceramic spacers between a top Al electrode and a water cooled Al ground plane. Both aluminum electrodes were lapped to minimize optical scattering losses. The upper electrode was divided into two segments which were separated by 6.0 mm. However, this separation was reduced to as small as 1.5 mm without producing any R.F. coupling between sections. The electrodes were covered by an Al_2O_3 plate to prevent corona of the low pressure gas near their surface. Each section was tuned and matched separately. When both sections were turned on, the impedance match for each was preserved. This result indicates the lack of electrical interaction between sections.

4.2 Operation and Behavior

When the laser was operated with a total input power of 200 watts, a maximum single mode output of 21 watts was obtained. The power versus pressure curves which are shown in Figure 4-3 were derived using a 84% reflector as the output coupler. Richer gas mixtures were also tested but they all yielded lower output powers.

The loss of power as the partial pressure of the carbon dioxide gas increases can be explained by considering the effect of helium on the gain of the waveguide laser. The measured gain coefficient as a function of the total gas pressure has been recorded by Abrams [22] and Lavigne et al. [26] for a variety of carbon dioxide gas mixtures. These curves display three main characteristics. First, the gain peaked at lower pressures for mixtures richer in carbon dioxide (greater than 10%). Secondly, the addition of He shifts the maximum gain towards higher pressures and lowers its maximum value; and finally, the gain coefficient is almost independent of pressure at high He concentrations. Therefore, if the distributed losses in the waveguide are reasonably large, a rich

FIGURE 4-3

Laser Output Power Versus Gas Pressure For Different He:CO_2:N_2:Xe Gas Mixtures; X: [16:1:2:0]; O: [15.2:1.9:1.9:1]. The Waveguide Cross Section was 2.5 mm Square.

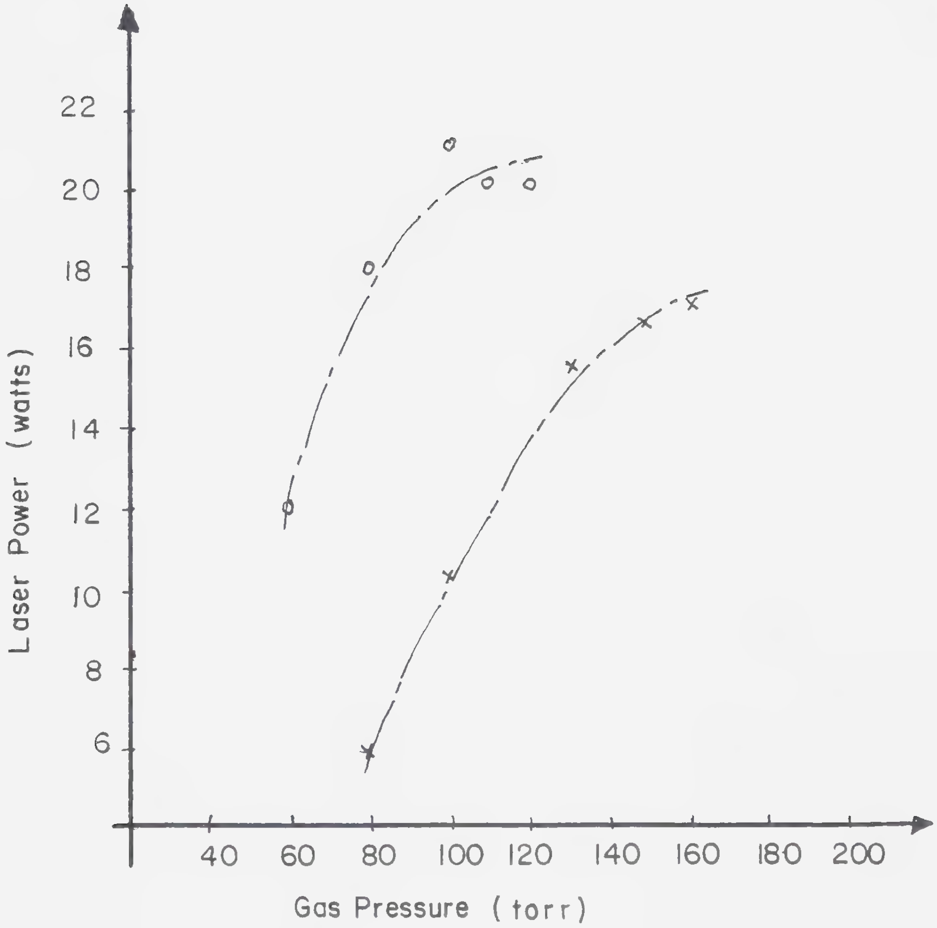

mix will not have sufficient gain at the higher pressures to produce population inversion. This behavior was precisely that which was observed. Lasing could only be achieved in the rich gas mixtures by lowering the gas pressure so that the gain would exceed the distributed loss.

Rich gas mixtures were also characterized by gaps which developed in the discharge at pressures greater than 100 Torr. This instability, as was discussed in the previous Chapter, arose because the input power density was not sufficient to maintain a positive impedance characteristic.

Since the waveguide channel was lossy, the output power versus reflectance, shown in Figure 4-4, was plotted to see if additional power could be obtained using a different output coupler. No additional power increase was obtained, however, as a lack of optics at 90% R, 80% R and 75% R prevented the accurate determination of this curve. The laser was also found to be extremely sensitive to alignment. With the 2.5 mm sq. bore, single mode operation was often difficult to achieve and maintain. This behavior was not improved even when a lossy output coupler such as a 60% reflector was used.

The channel size was reduced to a 2 mm sq. bore. This change increased the distributed loss (see Chapter 2) which lowered the maximum power to 19.5 watts when an 84% reflector was used. However, the alignment difficulties were reduced and the stability of the single mode output improved significantly. The power versus pressure curves for a 2 mm sq bore x 60 cm long waveguide are shown in Figure 4-5.

Although the power dropped slightly as the bore size decreased, the data obtained can still be shown to be in agreement with the scaling laws for carbon dioxide lasers [22]. As is well known, the gas pressure corresponding to the peak laser power multiplied by the tube diameter should be constant. Since the R.F.

FIGURE 4-4

Laser Output Power Versus Output Coupler Reflectance. A 2.5 mm sq Waveguide with a 14.8:2.1:2.1:1 [He:CO_2:N_2:Xe] Gas Mixture was Employed.

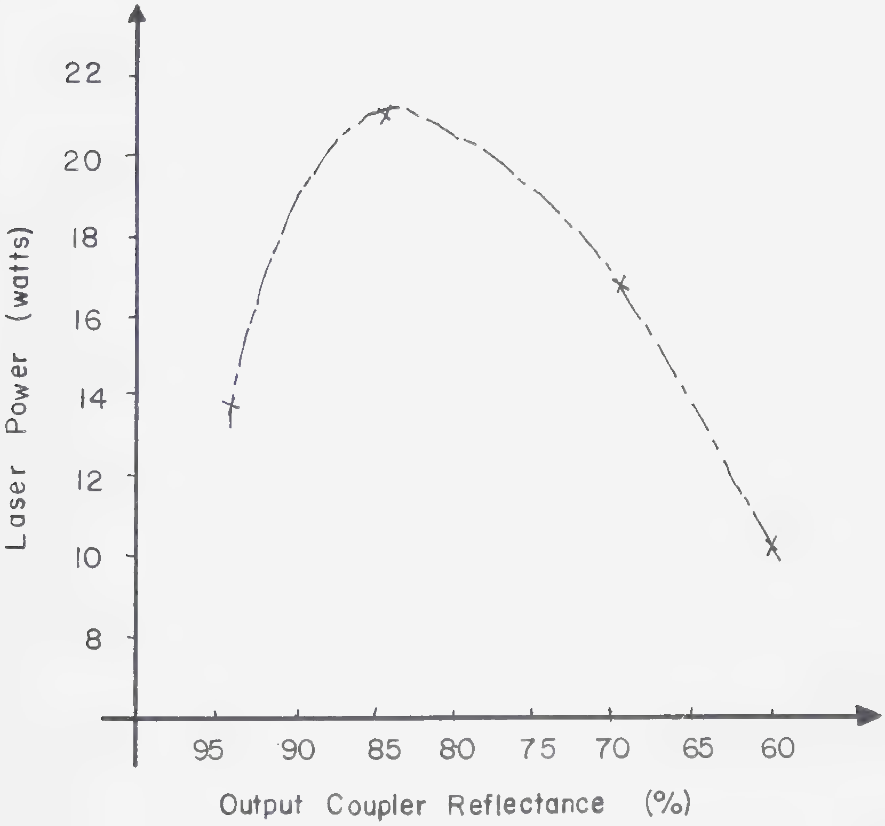

FIGURE 4-5

Laser Output Power Versus Gas Pressure For Different $He:CO_2:N_2:Xe$ Gas Mixtures; X: [14.8:2.1:2.1:1]; O: [13.6:2.7:2.7:1], △ : [15.5:1.7:1.7:1]. The Waveguide Cross Section was 2.0 mm Square.

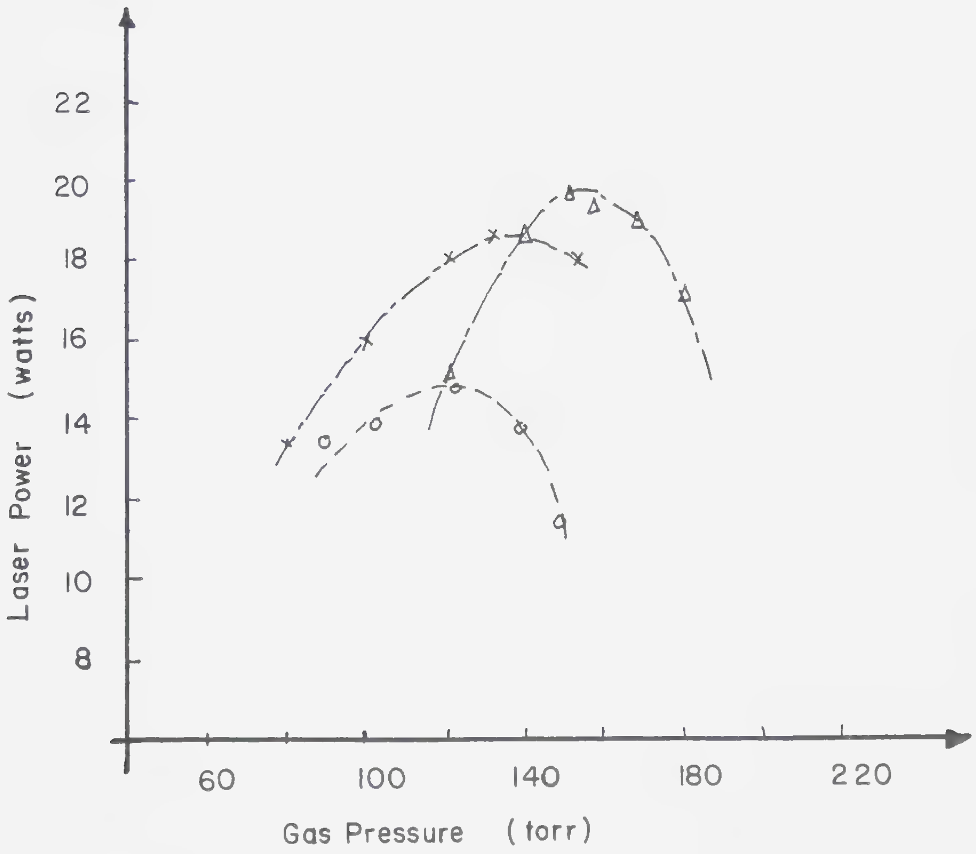

waveguide bore was square, the side wall dimension was used to represent the diameter. For a 2 mm sq. bore the maximum power occurred at 150 Torr, therefore, Pd = 30 Torr-cm. Similarly Pd = 30 for the 2.5 mm sq bore since the power peaked at 120 Torr. As expected the Pd product was constant.

The last characteristic to be examined is the laser efficiency. With a 2.5 mm sq bore a maximum of 21 watts of power was realized at an efficiency of 10.5%. With the 2.0 mm sq. bore the maximum output power of 19.5 watts was achieved at an efficiency of 9%. The loss of efficiency can most certainly be attributed to an increase in distributed losses (see Chapter 2). However, the question remains as to why only a maximum efficiency of 10.5% was realized when other researchers report efficiencies of 15% [49, 50].

The most important loss mechanism is optical scattering. Ideally the losses in the waveguide bore could have been measured using a stabilized CO_2 laser coupled into the guide with a lens. Such a laser was unavailable, however a visual examination of the channel revealed several potential sources of scattering. For example, six ceramic pieces were clamped together to form the channel. Scattering most certainly occurred at the discontinuities which were formed by slight misalignment of these pieces. Secondly, the channel surfaces were not polished smooth, but only lapped flat. Finally, the laser beam propagated through a salt window which sealed the vacuum envelope. This window was not anti reflection coated, therefore, both the inner and outer surface reflected a small percentage of the incident radiation.

Other potential loss mechanisms such as R.F. radiation and R.F. ohmic heating exist. A close examination of these mechanisms, however, indicated that their contribution was not significant.

As a final consideration, the laser cooling technique was examined to see if inadequate cooling of the gas mixture could account for the loss of efficiency. Several observations indicate that this was not the case. Firstly, the bottom electrode was water cooled. Secondly, the theoretical analysis (see Chapter 2) indicates that the gas should be adequately cooled. Thirdly, the laser was turned off and allowed to cool; when it was turned on again the laser power remained steady and did not decline as one would expect if the gas was being inadequately cooled.

The results presented in this Chapter indicate that a 20 watt 10% efficient laser is easily constructed. The discussion also indicates that the efficiency could be further increased if the optical quality of the channel was improved.

CHAPTER 5

THE FOLDED CAVITY DESIGN

5.1 Construction Details

One of the advantages of the R.F. excited CO_2 waveguide laser is its compact size. However, to maintain this advantage, when a high power CW output is required (greater than 20 watts), the optical cavity must be folded. Folded waveguide structures consisting of two or more parallel channels have been constructed by several researchers [63, 64]. The primary disadvantage of this arrangement is the optical loss which arises when the beam is steered from one channel to the other. To reduce this optical loss, the two channels are often orientated in a "v" shape [49, 65]. This orientation is superior because it only requires a single turn around optic so that the length of the unguided portion of the beam is minimized. For this reason a configuration consisting of a "v" shaped waveguide was adopted in the folded cavity design.

The remainder of the design was similar to the laser discussed in Chapter 4, except for a few improvements. The waveguide cross section was maintained at 2.5 mm sq, but the channel was a homogeneous alumina structure compared to the metal ceramic sandwich design previously employed. This homogeneous structure offered superior thermal stability which reduced guide bending and increased the transverse mode stability of the output beam.

As shown in Figure 5-1, the laser channel was formed by mounting 22 alumina pieces on two alumina slabs. Alternately the guide could have been formed using only four pieces of alumina, but such large pieces are very expensive. The upper reflecting surface was realized by clamping two cover plates to the top of this structure.

To reduce the optical scattering losses the interior surfaces of the waveguide were carefully polished prior to assembly. The bottom plates were first lapped using #500, #800 boron carbide abrasive and #1000 silicon carbide abrasive. These lapped surfaces were metallized using a Dupont Ag thick film paste [68] and polished using #600 emery paper, followed by tripoli and red rouge with a paraffin oil lubricant. The residues were removed by washing the plates for 15 minutes in an agitated bath of acetone. This metal thick film was used to enhance the reflectivity of the surface, to linearly polarize the laser beam, and to provide an electrical ground plane for the discharge. Alternately, the ground plane could have been established on the underside of the base plate, but such a configuration would have required a substantial voltage drop across the series capacitance provided by the bottom plate. As was discussed earlier (see Chapter 3), this additional voltage would raise the "Q" of the matching network and lead to greater resistive losses and electrical instability.

As was mentioned, the channel was formed by fastening the side pieces on the two bottom plates. These side pieces were originally metallized and soldered in place, however the resulting metal ceramic bonds were very weak and unreliable. Therefore, Torr Seal epoxy [69] was used to glue the waveguide side pieces to the base plates. The channel faces of the side pieces were also polished. After the boron and silicon abrasives were used, each section was polished using a 6 μm and a 1 μm diamond paste embedded in a polishing cloth. A light paraffin oil was used as a lubricant which enabled the polishing wheel to work unattended. Examination of the resultant optical finish with a scanning electron microscope revealed that all the remaining pits were less than 10 μm in diameter.

The top plate was lapped flat and clamped in place. The electrode, as shown in Figure 5-1b, was placed on the outside of the top alumina plate using an

FIGURE 5-1

The Photograph Below Shows the Waveguide Channel with the Matching Networks and the Top Ceramic Plates Removed. The Channel Was Formed with 22 Pieces of Al_2O_3 which were Mounted on Two 22.9 cm by 10.2 cm Pieces of Alumina. The Schematic Outlines the Cross-section of the Design in Greater Detail.

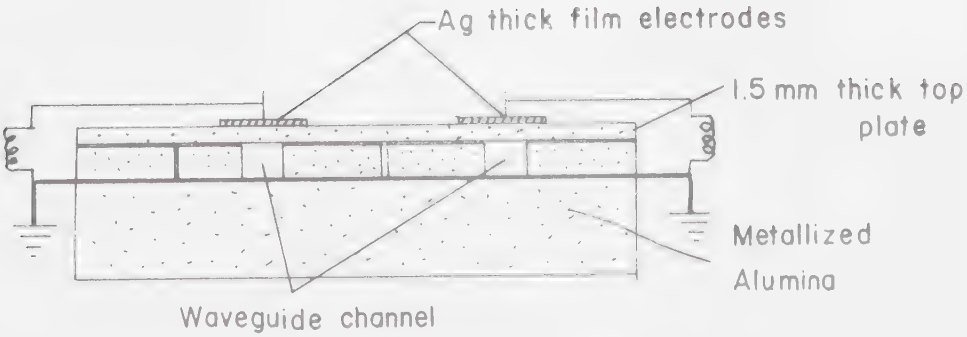

Ag thick film paste. From this electrode the R.F. energy was capacitively coupled through the top plate with a discharge then forming to ground. Originally the discharge side of the plate was also coated with a Pd/Ag layer to reduce the optical scattering losses. However, subsequent discharge tests indicated that this metal layer allowed R.F. standing voltages to develop.

One other important design improvement related to the input power density. The laser discussed in Chapter 4 was driven by two R.F. amplifiers, with each amplifier driving 30 cm of discharge. The folded cavity was driven with double the power, but each amplifier saw only 23 cm of discharge. Therefore, provided the gas mixture was not saturated, the laser was expected to produce twice the output power without doubling the length of the discharge.

As is shown in Figure 5-2, the remainder of the design was unchanged from the laser previously discussed. The laser was divided into four sections, each section was driven by a separate amplifier and resonated with three inductors. The mirrors were mounted 2 mm from the guide, and were externally adjustable. The laser was water cooled and an uncoated salt window was used to couple the radiation out of the vacuum envelope.

The Laser Operation

Initially only a single channel of the folded channel was aligned for laser operation. The single channel was constructed in two ways to assess the effects of a gap in the waveguide. The upper schematic in Figure 5-3 displays the guide of a single channel laser while the lower schematic displays the single guide geometry which originated in the double channel laser. When both geometries were tested, no differences in output power were observed. This result indicates that a one centimeter gap in the guide does not significantly increase the optical

FIGURE 5-2a

The Folded Cavity CO_2 Waveguide Laser

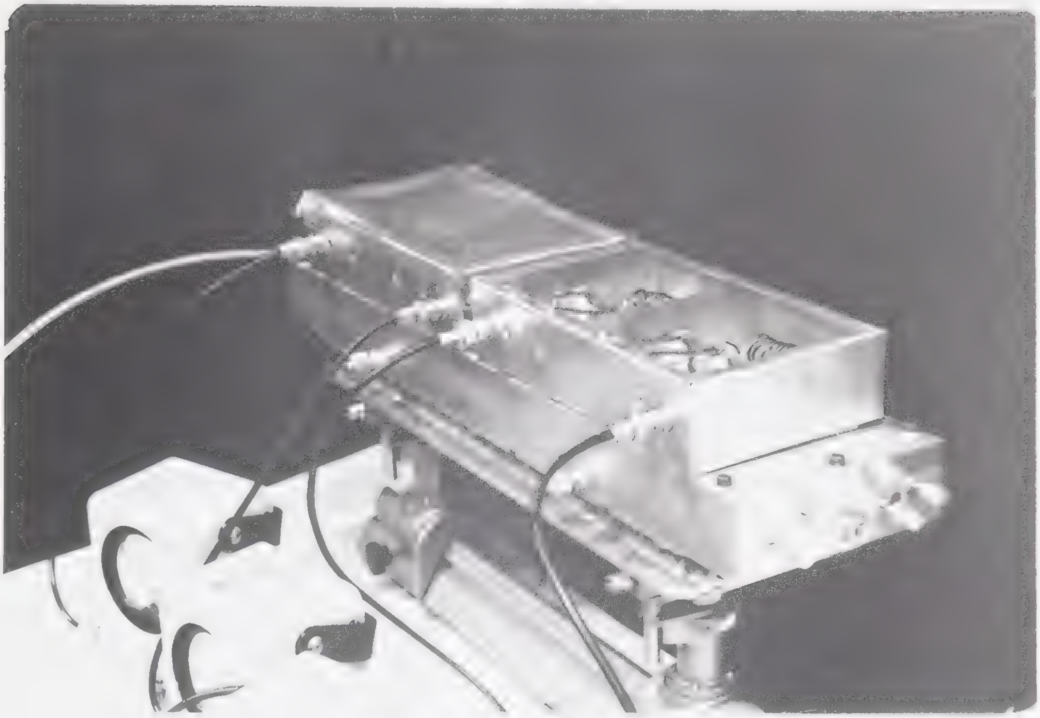

FIGURE 5-2b

An External View of the Waveguide Laser
With the Matching Networks Removed

FIGURE 5-3

Two Waveguide Geometries Which Were Aligned and Used as Single Channel Waveguide Lasers

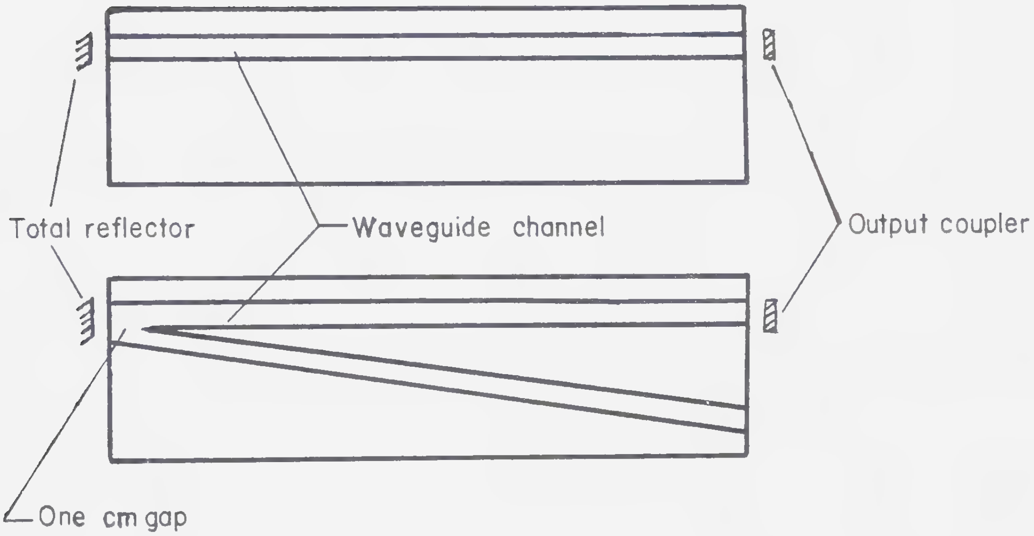

losses in the laser.

Early tests with this laser produced very low output powers. Mass spectroscopy analysis revealed that the acetone which was used to clean the channel was absorbed by the alumina. When the chamber was evacuated outgassing occurred which rapidly contaminated the carbon dioxide gas mixture. To avoid this contamination, the premix gas was flowed through the waveguide. With this arrangement the laser power rose from two to twelve watts while the discharge colour changed from gray to pink. The gas mixture, however, could not easily be optimized with a flowing gas arrangement, so the laser head was baked out at 80^{o} C for 15 hours. Subsequent operation yielded 12 watts with backfilled premix gas. This result indicated that the contamination problem had been eliminated. Further investigation indicated that this contamination problem could have been prevented by using a non-porous variety of alumina [38].

To compare a single channel of the folded cavity, to the 20 watt laser discussed in Chapter 4, an input power of 150 watts and an output coupler of 88% R was required to maintain the intracavity intensity at 125 watts. Since an 88% R output coupler was unavailable, an 84% R was used. The effect of gas mixture and gas pressure upon the output power is shown in Figure 5-4. Note that a maximum output power of 21 watts at 10% efficiency was obtained. With a slightly lower output power of 17.5 watts an efficiency of 11.6% was realized. This result compares favorably to the single channel laser discussed in Chapter 4. In addition, the output mode stability showed a substantial improvement.

The output power and laser efficiency versus input power are shown in Figure 5-5. The curve indicates that the gas mixture was not saturated, therefore, more than .46 watts/cm could be realized if more R.F. input power was

FIGURE 5-4

Laser Output Power Versus Gas Pressure For Three Different He:N_2:CO_2:Xe Gas Mixtures; X: [10:1:1: 0.6]; ☐ : [14:1.5:1:0.9]; O: [6:1:1:0.4]. A Single Channel Waveguide With 150 Watts of Input Power Was Used

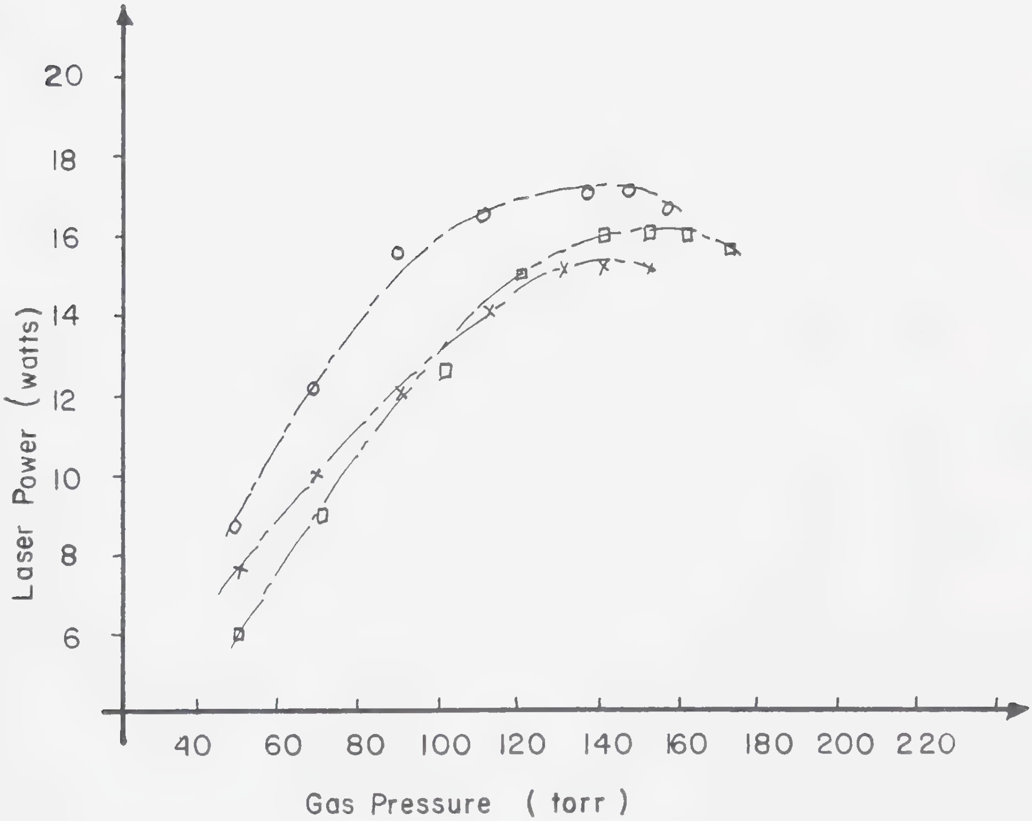

FIGURE 5-5

Laser Power (O) and Efficiency (X) Versus
Input Power For a Single Channel Laser

A $He:N_2:CO_2:Xe$ [6:1:1:0.4] Gas Mixture Was Used

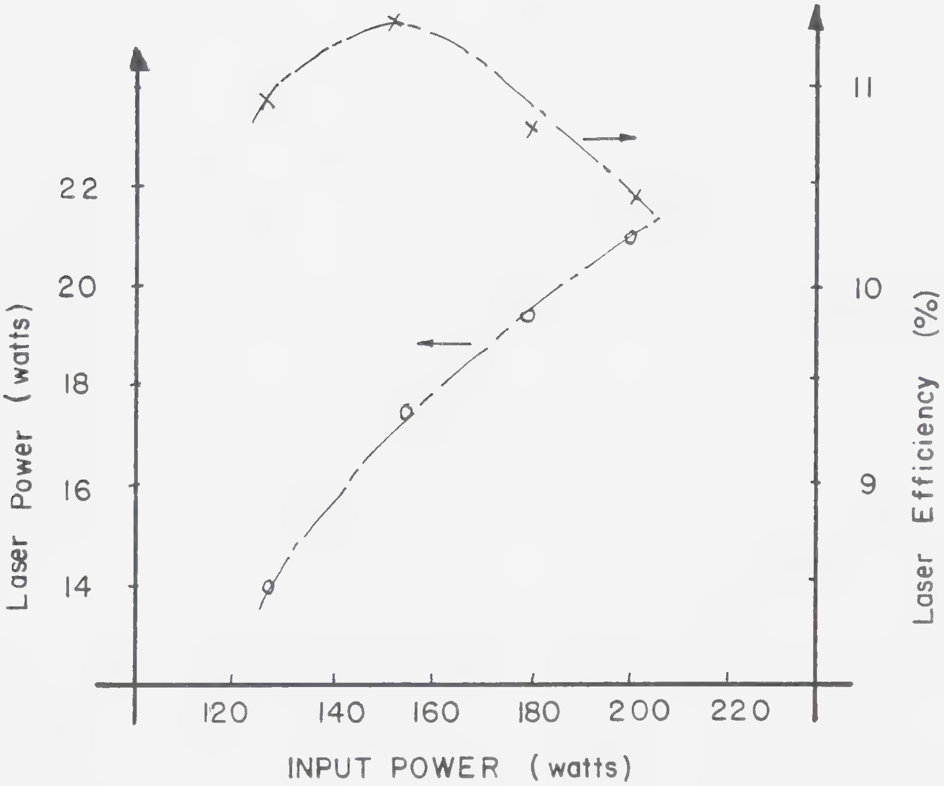

FIGURE 5-6

Laser Output Power Versus Gas Pressure For Different He N_2 CO_2 Xe Gas Mixtures;
O: [6:1:1:0.4]; X: [16:1:2:0]

The Input Power was 300 Watts into a Folded Cavity

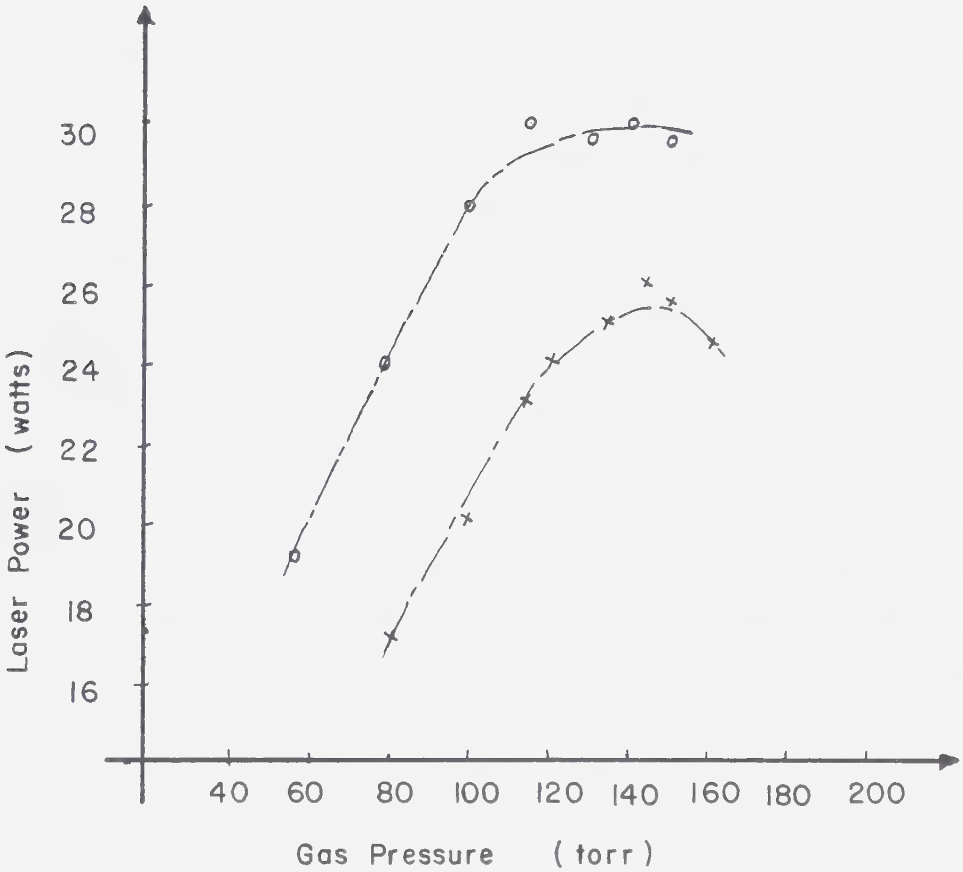

available. Further improvements in efficiency would also be possible if the salt window was antireflection coated and if the laser output coupler was better optimized.

When both channels were aligned, with an input power of 300 watts an output power of 30 watts was obtained. Figure 5-6 displays the laser power versus gas pressure curve for the double channel waveguide laser. Ideally this cavity should have produced 34 watts because a single channel produced 17 watts with an identical intracavity intensity. This power drop occurred because the folded cavity was much more difficult to align than the single pass system. To obtain a precise alignment the turn around optic had to be precisely located at the intersection point of the channel axis. Prealignment procedures with a HeNe laser indicated that the mirrors were not quite positioned correctly. This problem could have been corrected but not without a substantial investment of machine shop time. Overall however, the performance of the folded cavity laser was very encouraging. To further improve the laser operation several changes were possible. The mirror position could have been improved, the R.F. drive power increased, the output coupler could have been better optimized and the vacuum integrity of the guide improved. These improvements were not implemented to this laser because they could easily be incorporated along with other changes in a new design. These improvements, alternate designs and ideas for further work are discussed in greater detail in the next Chapter.

CHAPTER 6

CONCLUSIONS AND RECOMMENDATIONS

This thesis has examined the operation of waveguide lasers in detail, however, considerable research remains before a hard seal long life device can be constructed at the University of Alberta. The purpose of this chapter is to summarize the results presented in this work and to make suggestions for future work. The material will be discussed, to a large extent, in the same order as it was presented in the main body of the thesis.

Chapter 1 introduced waveguide lasers and outlined the advantages of these devices. Chapter 2 discussed the theoretical aspects of the design of waveguide lasers with special emphasis on laser cooling, optical losses and the optimum R.F. operating frequency.

Chapter 3 examined the results of the gas discharge experiments. A standing wave voltage was observed across the discharge, but was substantially reduced by positioning inductors along the electrode. The inductors added a positive phase contribution to cancel the negative phase contribution of the channel capacitance. The net effect was a more uniform discharge voltage. The laser discharge was matched to the R.F. amplifier with less than 1% reflected R.F. power. The minimum R.F. operating frequency to produce a stable discharge in a 2.5 to 2.0 mm sq bore waveguide was found to be about 40 MHz. More efficient excitation was realized by running at 70 MHz. The maximum operating frequency was found to depend upon the waveguide material and the required voltage uniformity. The realization of an optimum field/pressure ratio was shown to depend upon input power density and laser gas mix.

Chapter 4 examined the operation of a single channel hybrid carbon dioxide waveguide laser. With a 2.5 mm sq bore, the laser produced a maximum

of 21 watts at 10% efficiency. A smaller 2.0 mm sq bore laser yielded 19.5 watts at a reduced efficiency but the mode stability was observed to improve dramatically.

Chapter 5 discussed the operation of a folded cavity waveguide laser. Initially only a single pass of this structure was aligned. A maximum efficiency of almost 12% was easily realized. With 200 watts of input power, the laser still operated at over 10% efficiency. More importantly, the gas mixture was not saturated. Unfortunately a greater R.F. input power was not available to determine the maximum laser power that could be extracted from the gas mixture.

As a double pass laser, with 300 watts of input power, 30 watts of laser power was obtained. Clearly, the folded laser operation was superior to the single pass laser discussed in Chapter 4. This improvement was attributed to several factors. First, the reflecting surfaces of the guide were carefully polished to reduce the optical scattering losses. The guide was constructed entirely of alumina to reduce instabilities caused by thermally incompatible materials. The input power density was increased so that the gas mixture was more effectively excited. Finally, the guide was baked for 10 to 15 hours prior to use to ensure that all the impurities were removed from the vacuum envelope. Further gains in laser power and efficiency are projected by incorporating a few changes in a third design. In the following paragraphs these improvements are discussed.

To obtain efficient operation the waveguide should be constructed with a minimum number of carefully polished alumina strips. The alumina pieces should be non porous to reduce the possibility of contamination, and assembled to form a 2.5 mm sq bore waveguide. To estimate the optical scattering and absorption losses in the guide, a dither stabilized CO_2 laser beam could be propagated through the guide. This CO_2 laser could perhaps even be established as a

permanent facility to characterize any optical waveguide which is assembled.

Although 72 MHz was an acceptable operating frequency, an R.F. power supply operating at 100 or 150 MHz would be useful to obtain further insight into the effects of frequency upon efficient gas excitation. More importantly, the R.F. source should not oscillate below 72 MHz. Regardless of the operating frequency chosen, the maximum input power per centimeter of discharge should be substantially increased above 4.4 watts/cm so that the saturation power density can be identified. When the output power saturates the output coupler, reflectivity should be carefully optimized. Also, any external windows used to seal the vacuum envelope should be antireflection coated for 10.6 μm radiation.

If a folded cavity is required, the turn around optic should be precisely located at the intersection of the axis of the two channels. The optics can be mounted with adjusting screws but ideally they should be rigidly attached no farther than 2 mm from the guide.

The preceding discussion is at best only a brief outline of further work. The author believes, however, that these improvements will be sufficient to yield higher output powers (greater than 0.6 watts/cm) and greater efficiencies (up to 15%). The most challenging task though will be to maintain these specifications for greater than 1000 hours of operation. Lifetime studies of carbon dioxide waveguide lasers are currently being vigorously pursued in many research laboratories worldwide. This thesis has laid the groundwork, at the University of Alberta, by establishing the methodology required to build high output power (> 30 watts) CW carbon dioxide waveguide lasers, but much work remains. Hard sealing, refinement of cleaning and assembling techniques, combined with gas and lifetime studies must still be performed before a reliable laser source is obtained for surgical applications.

REFERENCES

1. Marcatili, E.A.J. and R.A. Schmeltzer, Bell System Tech. J., Vol. 43, No. 7, pp. 1783-1809, 1964.

2. Stefen, H. and E.K. Kneubuhl, Phys. Letters, Vol. 27A, No. 9, pp. 612-613, 1968.

3. Schwaller, P., H. Steffen, J.F. Moser and E.K. Kneubuhl, Appl. Optics, Vol. 6, No. 5, pp. 827-829, 1967.

4. Smith, P.W., Appl. Phys. Lett., Vol. 19, No. 5, pp. 132-134, 1971.

5. Bridges, T.J., E.G. Burkhardt and P.W. Smith, Appl. Phys. Lett., Vol. 20, No. 10, pp. 403-405, 1972.

6. Javan, A., Bennett, W.R., Herriot, D.R., Phys. Rev. Lett., Vol. 3, No. 3, pp. 106-110, 1961.

7. Laser Handbook Vol. 1, Ed. F.T. Arecchi, E.O. Schultz-Dubois, North Holland Amsterdam, pp. 623-626, 1972.

8. Barchewitz, P., L. Dorbec, R. Farrenq, A. Truffert and P. Vautier, C.R. Acad. Sci. (Paris), Vol. 260, pp. 3581, 1965.

9. Francis, G., Ionization Phenomena in Gases, Butterworth & Co., Toronto, pp. 81-172, 1960.

10. Crocker, A. and M.S. Willis, Electronic Lett., Vol. 5, No. 4, pp. 63-64, 1969.

11. Brown, C.O. and J.W. Davis, Appl. Phys. Lett., Vol. 21, No. 10, pp. 480-481, 1972.

12. Nichols, D.B. and W.M. Brandenberg, IEEE J. Quantum Electron., Vol. QE-9, No. 8, pp. 718-719, 1973.

13. Lachambre, J.L., J. MacFarlane, G. Otis and P. Lavigne, Drev M-2446/78, 1978.

14. Laakmann, K.D. and D. Matz, Conference on Laser Engineering Applications, Washington, D.C., 1977, paper 6.10.

15. Laakmann K.D., US Patent Number 4,169,251 (assigned to Hughes Aircraft Co.), Sept. 25, 1979.

16. Laakmann, K.D., Transverse R.F. Excitation for Waveguide Lasers, presented at the International Conference on Lasers, 1978, Orlando, FL.

17. Mittelman, H., A. Vassiladis, K. Laakmann and P. Laakmann, American Society for Lasers in Medicine and Surgery. January 27, 1981.

18. Lobraico, R.V., International Congress on Applications of Lasers and Electro-optics, Boston, Sept. 20-23, 1982. Paper 1B-9.

19. Abrams, R.L., Laser Handbook Volume 3, Ed. M.L. Stitch, North Holland Publishing Co., Amsterdam, pp. 41-88, 1979.

20. Rigrod, W.W., J. Appl. Phys., Vol. 36, No. 8, pp. 2487-2490, 1965.

21. Matsumoto, K., H. Shirahata and T. Fujioka, IEEE J. Quant. Electronics, Vol. QE-14, No. 10, pp. 781-782, 1978.

22. Abrams, R.L. and W.B. Bridges, IEEE J. Quantum Electronics, Vol. QE-9, No. 9, pp. 940-946, 1973.

23. Burkhardt, E.G., T.J. Bridges and P.W. Smith, Optics Comm., Vol. 6, No. 2, pp. 193-195, 1972.

24. J.P. Holman, Heat Transfer, McGraw Hill Book Co., New York, NY, pp. 20-27, 1963.

25. Christensen, C.P., F.X. Powell and N. Djeu, IEEE J. Quantum Electronics, Vol. QE-16, No. 9, pp. 949-954, 1980.

26. Lavigne, P., G. Otis and D. Vincent, Performance Characteristics of a CO_2 Waveguide Laser, Drev R-4150/79, 1979.

27. Papayoanou, A., Ecom. Tech. Report No. 4430, Sept. 1976.

28. Laakmann, K.D. and W.H. Steier, Appl. Optics, Vol. 15, No. 5, pp. 1334-1340, 1976.

29. Rosebury, F., Handbook of Electron Tube and Vacuum Techiques, Addison Wesley, Mass., 1965.

30. Kohl, W.H., Handbook of Materials and Techniques for Vacuum Devices, Reinhold Publishing Corp., New York, 1967.

31. Union Carbide Corporation Technical Information Bulletin #442-217.

32. Loh, E., Physical Review, Vol. 166, No. 3, p. 673, 1968.

33. Gielisse, P.J., S.S. Mitra, J.N. Plendl, R.D. Griffis, L.C. Mansur, R. Marshall and E.A. Pascoe, Physical Review, Vol. 155, No. 3, pp. 155, 1967.

34. Gorton, E.K. and J.R. Redding, J. Phys. E. Sci. Instrum., Vol. 13, pp. 335-340, 1980.

35. Physics Handbook, Ed. D. Gray, McGraw Hill Book Co., New York, NY, 6-118, 6-153, 1972.

36. Abrams, R.L., Interim Tech. Report, ONR Contract No. N0014-73-C-0324, NTIS #AD-769-067, October, 1973.

37. Laakmann, K.D. and P. Laakmann, SPIE, Vol. 247, pp. 74-78, 1980.

38. Private Communication, P. Tarnowski, Coors Porcelain, Golden, CO, 1982.

39. Garmire, E., T. McMahon and M. Bass, Applied Optics, Vol. 15, No. 1, pp. 145-150, 1976.

40. Private Communication, P. Pace, Defence Research Establishment: Valcartier, Quebec, November 1982.

41. Avrillier, S. and J. Verdonck, J. Appl. Phys., Vol. 48, No. 12, pp. 4937-4941, 1977.

42. Garmire, E., T. McMahon and M. Bass, IEEE J. Quantum Electron., Vol. QE-16, No. 1, pp. 23-32, 1980.

43. Hall, D.R., R.M. Jenkins and E.K. Gorton, J. Phys. D., Vol. 11, pp. 859-969, 1978.

44. Waksberg, A.L., A.C. Boac and S. Sizgoric, IEEE J. Quantum Electron., Vol. QE-7, No. 1, pp. 29-35, 1971.

45. Volskaya, S.P., V.I. Pugnin, A.I. Tselykovskii and V.A. Stepanov, J. of Appl. Spectroscopy, Vol. 35, No. 2, pp. 138-142, 1981.

46. Griffith, G.A., U.S. Patent #4,352,188 (assigned to Hughes Aircraft Co.), September 25, 1982.

47. Griffith, G.A., SPIE Vol. 270, CO_2 Laser Devices and Applications, pp. 6-11, 1980.

48. Lachambre, J.L., J. MacFarlane, G. Otis and P. Lavigne, Appl. Phys. Lett., Vol. 32, No. 10, pp. 652-653, 1978.

49. Chenausky, P.P., R.A. Hart, L.A. Newman and N.M. Hoffman, CLEOS Paper #THN2, 1982.

50. Sutter, L.V., SPIE, Vol. 227, CO_2 Laser Devices and Applications, pp. 2-5, 1980.

51. Johnson, J., Solid Circuits, Circuit Techniques, Book #2280A, Communications Trans. Corp., San Carlos, CA, 1962.

52. DuPont Thick Film Products Brochure No. E-33368, 1980.

53. Hill, R.A., C.F. Brown, G.A. Griffith, L.V. Sutter, F.A. Douezal, R.D. Washburn and E.R. Peresshi, SPIE, Vol. 227, CO_2 Laser Devices and Applications, pp. 12-16, 1980.

54. Hecht, J., Lasers and Applications, Vol. 1, No. 1, p. 85, 1982.

55. Allcock, G. and D.R. Hall, Optics Comm., Vol. 37, No. 1, pp. 49-52, 1981.

56. Davis, Matching Network Design with Computer Solutions, Motorola Application Note AN-267.

57. Lowke, J.J., A.V. Phelps and B.W. Irwin, J. Appl. Phys., Vol. 44, No. 10, pp. 4664-4671, 1973.

58. Ishchenko, V.N., V.N. Lisitsyn, V.P. Safonov and A.R. Sorokin, Sov. J. Quantum Electron., Vol. 5, No. 7, pp. 738-741, 1975.

59. Christensen, C.P., App. Phys. Lett., Vol. 34, No. 3, pp. 211-213, 1979.

60. Cohn, D.B., App. Phys. Lett., Vol. 37, No. 9, pp. 771-773, 1980.

61. Generalov, N.A., V.P. Zimakov, V.D. Kosynkin, Yu. P. Raizer and D.I. Roitenburg, Sov. J. Plasma Phys., Vol. 3, No. 3, pp. 354-358, 1977.

62. DeMaria, A.J., Proceedings of the IEEE, Vol. 61, No. 6, pp. 731-748, 1973.

63. Marcus, S. and J.W. Caunt, Rev. Sci. Instruments, Vol. 79, No. 10, pp. 1410-1412, 1978.

64. Mocker, H.W., Miniaturized CO_2 Waveguide Laser, SPIE, Vol. 227, pp. 17-22, 1980.

65. Whitebook, M.E., P. Laakmann and K.D. Laakman, CLEO, 1980, paper THQ2.

66. Nimsakul, N., in Lasers in Medicine, Vol. 1, H.K. Koebner, ed., John Wiley and Sons, New York, NY, p. 126, 1980.

67. Carter, G.M. and S. Marcus, App. Phys. Lett., Vol. 35, No. 2., pp. 129-130, 1979.

68. Dupont thick film is a metal glass paste which is painted on the alumina surface and processed at 850°C for ten minutes in air. During the firing process the organic carrier is burnt off while a frit bond is formed between the glass and the ceramic. This technique is relatively easy to use but the resulting bond is very sensitive to leaching when soldered.

69. "Torr Seal" is a low vapour pressure adhesive designed specifically for use in vacuums as low as 10^{-8} torr. Therefore, contamination via outgassing will not be a problem.

70. Abrams, R.L., IEEE J. of Quantum Electronics, Vol. QE-8, No. 11, pp. 838-843, 1972.